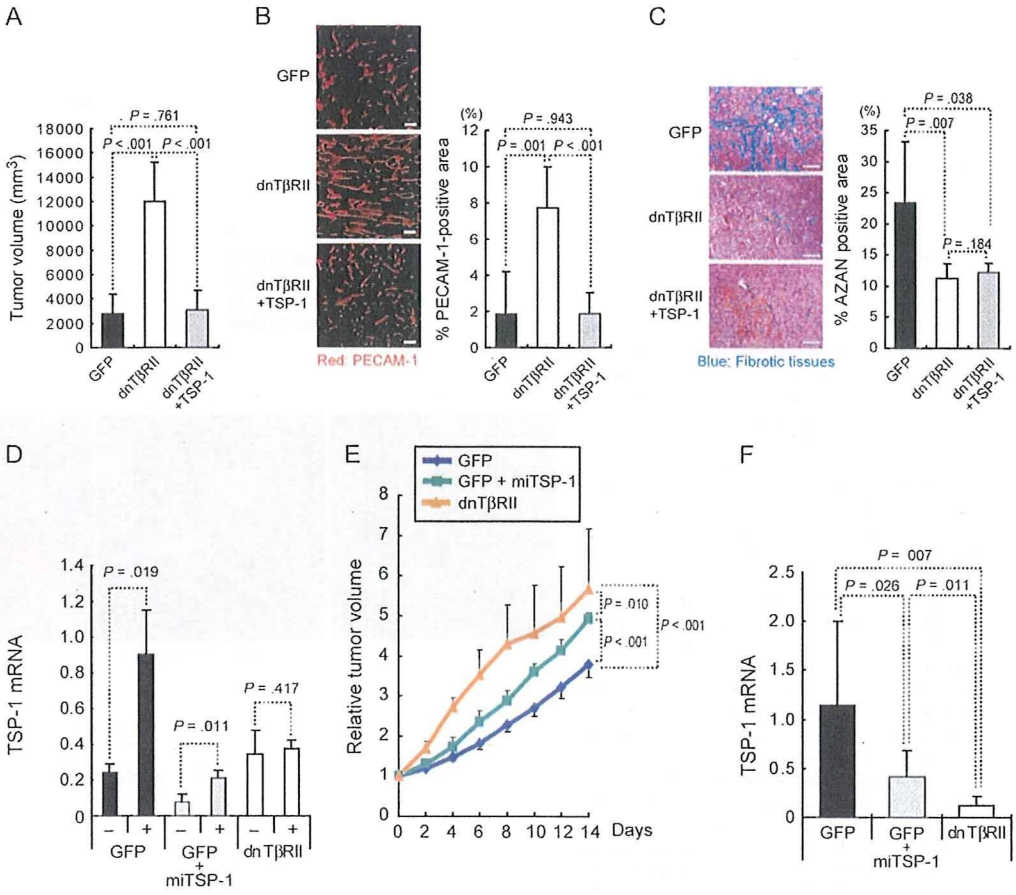

Figure 4. Expression of TSP-1 and tumor growth in nude mice. **A)** Tumor volume and TSP-1 expression. The 2MLN-dnTβRII cells, which stably express TSP-1, are termed 2MLN-dnTβRII+TSP-1. Volumes of the subcutaneous tumors produced by 2MLN-GFP, 2MLN-dnTβRII, and 2MLN-dnTβRII+TSP-1 cells were determined 7 days after inoculation (n = 6 mice per group). **B)** Vascular density at 7 days after inoculation as determined by immunostaining for PECAM-1. **Left)** Immunostaining with antibody against PECAM-1. Scale bars = 100 μm. **Right)** Percent PECAM-1–positive area (n = 3 with each condition). **C)** Fibrotic tissue as determined by AZAN staining in the subcutaneous tumors 7 days after inoculation. **Left)** Micrographs with fibrotic tissue stained **blue** by AZAN staining. Scale bars = 100 μm. **Right)** Percent AZAN-positive area (n = 3 with each condition). **D)** The effect of miTSP-1 mRNA expression in the gastric cancer cells as determined by TSP-1 mRNA expression. The 2MLN-GFP, 2MLN-GFP+miTSP-1, and 2MLN-dnTβRII cells were treated with TGF-β or left untreated for 24 hours in vitro, and expression of TSP-1 mRNA was compared among the cell lines. The experiment was conducted two times, each sample was assayed in triplicate, and data were averaged. Data from one representative experiment are shown. **E)** Growth curves of 2MLN-GFP, 2MLN-GFP+miTSP-1, and 2MLN-dnTβRII xenograft tumors in nude mice (n = 6 in each condition). In 2MLN-GFP+miTSP-1 cells, the expression of TSP-1 was reduced by use of the miTSP-1. Tumor volume is shown relative to the average volume in each condition at day 0 after starting evaluation. **F)** Expression of TSP-1 mRNA in the 2MLN-GFP, 2MLN-GFP+miTSP-1, and 2MLN-dnTβRII tumors in vivo. Experiment was conducted two times, each sample was assessed in triplicate, and data were averaged. Data from one representative experiment are shown. **Error bars** = 95% confidence intervals. All *P* values (two-sided), except for those in **(E)**, were calculated using the Student's *t* test. *P* values in **(E)** were calculated by two-way repeated measures analysis of variance. dnTβRII = dominant-negative TGF-β type II receptor; miTSP-1 = microRNA against thrombospondin-1; GFP = green fluorescent protein; TGF-β = transforming growth factor β; TSP-1 = thrombospondin-1; PECAM-1 = platelet–endothelial cell adhesion molecule-1.

which were obtained under a blanket written informed consent. Tissue sections were prepared from paraffin blocks and then incubated in antigen retrieval solution (Histo VT one; Nacalai Tesque, Kyoto, Japan) at 105°C for 20 minutes for thrombospondin-1 and for 40 minutes for phosphorylated Smad2. Sections were immunostained with primary and secondary antibodies. The primary antibodies used were rabbit anti-phosphorylated Smad2 monoclonal antibody and mouse anti-thrombospondin-1 monoclonal antibody. Secondary antibodies used were Alexa 488–conjugated goat anti-rabbit IgG antibody and/or Alexa 594–conjugated goat anti-mouse IgG antibody and were visualized by use of a Zeiss LSM510 Meta confocal microscope (Thornwood, NY) for immunohistochemistry and GFP fluorescence, and with an Olympus (Tokyo, Japan) AX80 microscope for hematoxylin–eosin and AZAN staining. Sections were scored positive when more than approximately 10% of the cancer cells were moderately or strongly stained, according to a recent study (27). In control experiments, the primary antibodies were omitted.

Statistical Analyses

Results were analyzed statistically by two-sided Student's *t* tests or by two-way repeated measures analysis of variance (ANOVA) tests with JMP6 software (SAS Institute, Raleigh, NC), where applicable. Results of immunohistochemistry for human surgical samples were analyzed with the χ^2 test. Results were considered to be statistically significant at $P < .05$. All statistical tests were two-sided.

Results

Disruption of TGF-β Signaling and Growth of Xenografted Tumors in Mice

We investigated the role of TGF-β signaling in human diffuse-type gastric carcinoma by transfecting OCUM-2MLN cells with lentiviral constructs expressing dnTβRIIs or a GFP control. We first determined whether the parental OCUM-2MLN cells and transfected 2MLN-GFP and 2MLN-dnTβRII cells respond to TGF-β in vitro by expressing GFP or dnTβRII, by use of

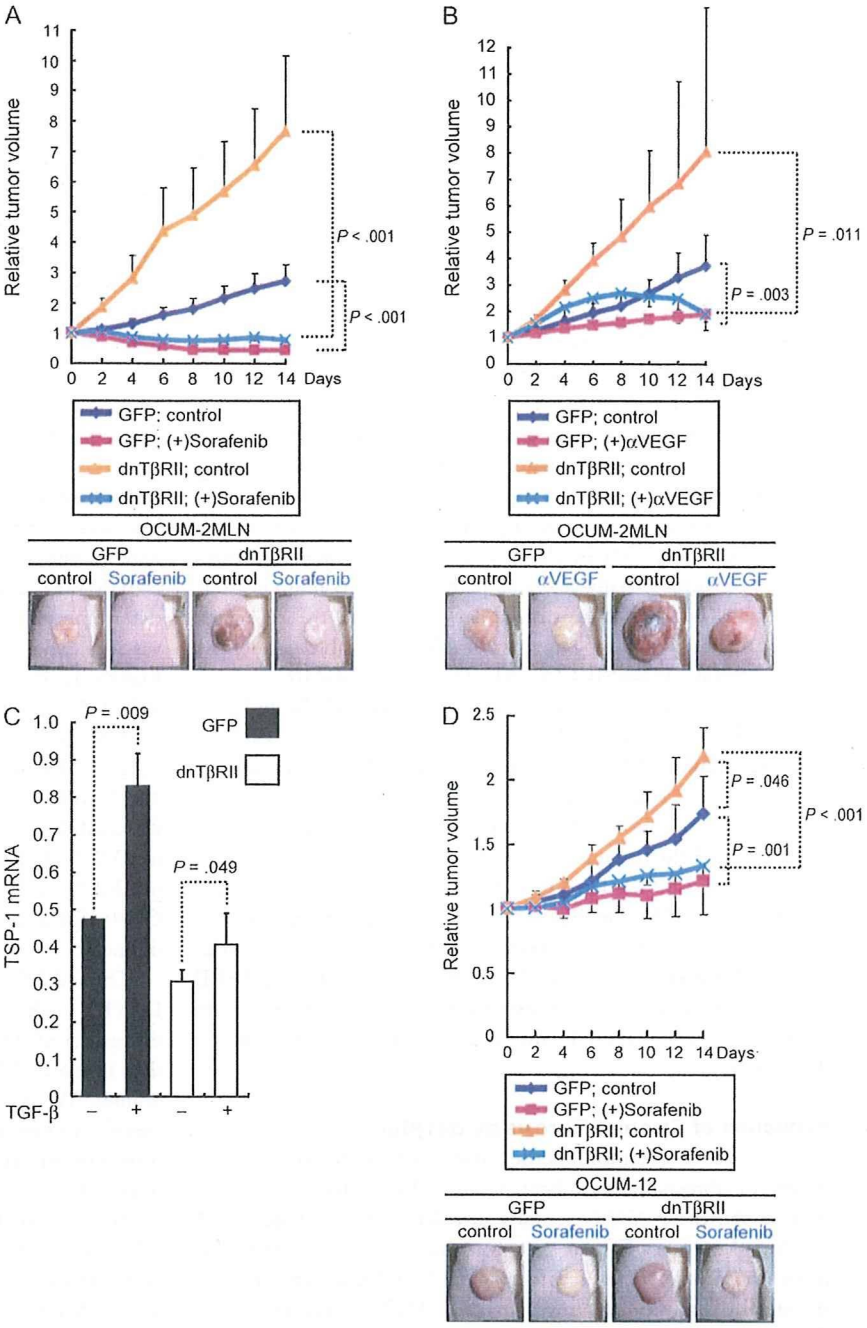

Figure 5. Administration of sorafenib and tumor growth in nude mice. **A)** Growth curve of xenografted 2MLN-GFP and 2MLN-dnTβRII tumors and sorafenib treatment. Mice bearing tumors were treated with 800 μg of sorafenib or with vehicle, as indicated, every day for 14 days (n = 6 mice per group). The representative macroscopic appearance of the tumors at day 7 is shown in the **bottom panels. B)** Growth curve of xenografted 2MLN-GFP and 2MLN-dnTβRII tumors in the presence and absence of anti-VEGF neutralizing antibody (n = 6 mice per group). Mice bearing tumors were treated for 14 days with 50 μg of anti-VEGF antibody or vehicle, as indicated, twice a week. The representative macroscopic appearance of the tumors at day 7 is shown in the **bottom panels. C)** Expression of human TSP-1 mRNA and treatment with TGF-β. TSP-1 mRNA expression was determined by quantitative real-time reverse transcription–polymerase chain reaction in the control OCUM-12-GFP (GFP) and OCUM-12-dnTβRII (dnTβRII) cells that were treated with TGF-β (1 ng/mL) or left untreated for 24 hours in vitro. The experiment was conducted two times, each sample was assessed in triplicate, and data were averaged. Data from one representative experiment of these are shown. **D)** Growth curves of xenografted OCUM-12-GFP and OCUM-12-dnTβRII tumors and sorafenib treatment. Mice bearing tumors were treated with 800 μg of sorafenib or with vehicle, as indicated, every day for 14 days (n = 7 mice per group). The representative macroscopic appearance of the tumors at day 14 is shown in the **bottom panels. Error bars** = 95% confidence intervals. *P* values for **(A)**, **(B)**, and **(D)** were calculated by two-way repeated measures analysis of variance. Those for **(C)** were calculated with a Student's *t* test, two-sided. DMSO = dimethyl sulfoxide (vehicle). dnTβRII = dominant-negative TGF-β type II receptor; GFP = green fluorescent protein; VEGF = vascular endothelial growth factor; TGF-β = transforming growth factor β; TSP-1 = thrombospondin-1.

immunoblotting. We found that GFP was expressed in the 2MLN-GFP control cells and dnTβRII was expressed in 2MLN-dnTβRII cells (Figure 1, A). In contrast to the parental 2MLN cells and GFP-transfected 2MLN-GFP cells, TGF-β–induced phosphorylated Smad2 was not detected in 2MLN-dnTβRII cells (Figure 1, A). We next used quantitative real-time RT-PCR analysis to show that the induction of Smad7 mRNA, a well-known target of TGF-β signaling, by TGF-β was lower in the 2MLN-dnTβRII cells than in OCUM-2MLN or 2MLN-GFP cells (Figure 1, B). 2MLN, 2MLN-GFP, and 2MLN-dnTβRII cells had similar proliferation rates, and the proliferation rates of these cells were not statistically significantly inhibited after TGF-β treatment (Figure 1, C).

Next, 2MLN-GFP or 2MLN-dnTβRII cells were subcutaneously transplanted into nude mice (n = 8 mice in each group), and tumor size was measured every other day until day 10. Although the proliferation of these cell types did not differ in vitro, the volumes of 2MLN-dnTβRII tumors were statistically significantly larger than those of 2MLN-GFP tumors (Figure 1, D; mean volume on day 10 relative to that on day 0 of 2MLN-dnTβRII tumors = 3.49 and of 2MLN-GFP tumors = 2.46, difference = 1.02, 95% confidence interval [CI] = 0.21 to 1.84; for group effect, $P = .003$;

and for the sampling time effect and the dnTβRII group effect × sampling time effect, $P < .001$, by a two-way repeated measures ANOVA test for tumor growth). We also orthotopically transplanted 2MLN-GFP or 2MLN-dnTβRII cells into the gastric wall of nude mice and determined tumor size on days 14 and 21 after implantation. The relative tumor area of 2MLN-dnTβRII (2.98) was statistically significantly larger than that of 2MLN-GFP (1.59) (Figure 1, E) (difference = 1.39, 95% CI = 0.87 to 1.91; $P < .001$, n = 8 mice in each group).

To explore factors responsible for the increased growth of the 2MLN-dnTβRII tumors in vivo, we used microarray analysis to identify differentially expressed human genes in the subcutaneously transplanted 2MLN-GFP and 2MLN-TβRII tumors and then used pathway analysis with the DAVID program to annotate the list of differentially expressed genes in these tumors. The DAVID program provides batch annotation and gene ontology term enrichment analysis to highlight the most relevant gene ontology terms associated with a given gene list (26). The analysis of our microarray data by the DAVID program identified three pathways as differentially activated pathways: cell communication, interactions between the extracellular matrix and the receptors, and focal adhesion (Supplementary Table 2, available online). All three pathways included *COL1A1*, *THBS1*, and *LAMC2*, whose expression levels were substantially lower in 2MLN-dnTβRII tumors than in 2MLN-GFP tumors (Supplementary Table 2, available online). *COL1A1* encodes procollagen I, which is involved in fibrosis, and *THBS1* encodes thrombospondin-1, which is an angiogenesis inhibitor. *LAMC2* encodes laminin-γ2 and was also included in all the three pathways. Although the increased expression of laminin-γ2 has been reported to be involved in invasion of certain cancers (28), the importance of its decreased expression in cancer remains unknown. Therefore, we further analyzed the relationship between the increased growth of the 2MLN-dnTβRII tumors and tumor microenvironment, especially fibrosis, with a focus on procollagen I, and angiogenesis, with a focus on thrombospondin-1.

Reduction of Stromal Fibrosis by dnTβRII

We analyzed the tumor microenvironment by determining the degree of fibrosis in the subcutaneous and orthotopic tumor tissues, as shown by AZAN staining of collagen fibers (Figure 2, A and Supplementary Figure 1, A, available online). In both tumor types, the area of fibrosis as determined by AZAN staining was statistically significantly lower in the 2MLN-dnTβRII tumors than in the 2MLN-GFP tumors (for subcutaneous tumors, 2MLN-dnTβRII had 6.1% and 2MLN-GFP had 30.1% [n = 9 mice per group], difference = 24.0%, 95% CI = 14.4% to 33.6%, $P < .001$; and for orthotopic tumors, 2MLN-dnTβRII tumors had 19.8% and 2MLN-GFP tumors had 47.0%, n = 9, difference = 27.2%, 95% CI = 20.0% to 34.4%, $P < .001$).

Microarray analysis revealed that the COL1A1 expression was lower in the 2MLN-dnTβRII tumors than in the 2MLN-GFP tumors. These results were validated with quantitative real-time RT-PCR with human COL1A1–specific primers and subcutaneous tumor samples (expression in 2MLN-dnTβRII tumors was 1.01 arbitrary units and that in 2MLN-GFP tumors was 17.46 arbitrary units, n = 3, difference = 16.4, 95% CI = 12.3 to 20.6 arbitrary units, $P < .001$) (Figure 2, B, left panel). In the same tumors, expression of the mouse Col1A1 mRNA was similar in 2MLN-dnTβRII and 2MLN-GFP tumors (Figure 2, B, middle panel; $P = .026$). In cultured cells, expression of the human COL1A1 mRNA was induced by TGF-β in the 2MLN-GFP cells but not in the 2MLN-dnTβRII cells (Figure 2, B, right panel). Secretion of TGF-β1 as determined by an enzyme-linked immunosorbent assay revealed that production of TGF-β1 was lower in 2MLN-dnTβRII cells (22.1 pg/mL) than in 2MLN-GFP cells (552.4 pg/mL) (difference = 530.3 pg/mL, 95% CI = 502.7 to 558.0 pg/mL, $P < .001$) (Figure 2, C). Thus, the material in the extracellular matrix in these tumors appears to be derived primarily from the gastric carcinoma cells and that the increased production of these extracellular matrix materials may be induced by TGF-β1 that is produced by the gastric carcinoma cells.

Induction of Tumor Angiogenesis by dnTβRII

We next examined tumor angiogenesis, another important component of the tumor microenvironment, in 2MLN-dnTβRII and 2MLN-GFP tumors in vivo. We used immunohistochemistry to determine vascular density in tumors with a specific marker of vascular endothelium, PECAM-1 (Figure 2, D and Supplementary Figure 1, B, available online). In subcutaneous tumors, the PECAM-1–positive area was statistically significantly higher in 2MLN-dnTβRII tumors (8.91% per microscopic field) than in 2MLN-GFP tumors (4.78%) (n = 6, difference = 4.13%, 95% CI = 1.31% to 6.94%; $P = .008$) (Figure 2, D). In orthotopic tumors, the PECAM-1–positive area was also statistically significantly higher in 2MLN-dnTβRII tumors (1.95% per microscopic field) than in 2MLN-GFP tumors (0.27%) (n = 7, difference = 1.67%, 95% CI = 0.46% to 2.88%; $P = .013$) (Supplementary Figure 1, B, available online).

The *THBS1* gene was included in all pathways selected by DAVID analysis, and the microarray analysis showed that the expression of THBS1 was lower in the 2MLN-dnTβRII tumors than in the 2MLN-GFP tumors (Supplementary Table 2, available online). We used quantitative RT-PCR with human THBS1–specific primers to confirm that the expression of THBS1 mRNA from human carcinoma cells was lower in the 2MLN-dnTβRII tumors (0.13 arbitrary unit) than in the 2MLN-GFP tumors (2.20 arbitrary units) (difference = 2.07 arbitrary units, 95% CI = 1.92 to 2.22 arbitrary units; $P < .001$) (Figure 2, E, left panel). Moreover, expression of thrombospondin-1 was potently induced by TGF-β in the 2MLN-GFP cells in vitro but not in the 2MLN-dnTβRII cells (Figure 2, E, right panel). In addition to thrombospondin-1, VEGF has been reported to be involved in angiogenesis in the Smad4-deficient pancreatic tumor model (29). However, the level of VEGF expression, as determined with primers specific for both human and mouse VEGF, was similar between 2MLN-GFP and 2MLN-dnTβRII cells in vivo and in vitro (data not shown), indicating that decreased expression of thrombospondin-1 may be involved in the enhanced angiogenesis in the 2MLN-dnTβRII tumors.

Phenotype of Tumors Containing a Mixture of Both 2MLN-GFP and 2MLN-dnTβRII Cells

The results described above strongly suggest that regulation of structural elements in the tumor microenvironment by TGF-β

signaling may be important to tumor formation in diffuse-type gastric carcinomas; however, it is still possible that the changes in tumor growth rate may be induced by other autonomous factor(s) in the cancer cells. To investigate further whether the tumor microenvironment serves as a major determinant of tumor growth in this model, we mixed equal amounts of the 2MLN-GFP and 2MLN-dnTβRII cells and transplanted the cell mixture into nude mice (Figure 3, A). If the tumor microenvironment plays a major role in tumor growth, then the 2MLN-GFP+dnTβRII tumors should contain equal number of both cell types (Figure 3, A). In contrast, if the 2MLN-dnTβRII portion of the tumor grows faster in cell-autonomous fashion, then the 2MLN-GFP+dnTβRII tumors should be composed mainly of 2MLN-dnTβRII cells. Histological examination of 2MLN-GFP+dnTβRII tumors with GFP fluorescence and by use of hemagglutinin antibody to detect the 2MLN-GFP and 2MLN-dnTβRII cells, respectively, revealed that the 2MLN-GFP+dnTβRII tumors contain almost equal number of the two cell types ($P = .56$) (Figure 3, B). We also examined angiogenesis in 2MLN-GFP+dnTβRII tumors by use of PECAM-1 immunostaining and found that the level of vascular density in the mixed-cell tumor (2.61% per microscopic field) was intermediate between that of 2MLN-dnTβRII tumors (4.22%) and 2MLN-GFP tumors (1.34%) (difference with 2MLN-dnTβRII tumors = 1.61, 95% CI = 0.37% to 2.86%, $P = .023$ [n = 3]; difference with 2MLN-GFP tumors = 1.27%, 95% CI = 0.73% to 1.81%, $P = .003$ [n = 3]) (Figure 3, C).

Inhibition of Angiogenesis and Growth of 2MLN-dnTβRII Tumors

To determine whether decreased thrombospondin-1 expression is involved in the accelerated proliferation of 2MLN-dnTβRII tumors, we used a lentivirus system to introduce the gene for thrombospondin-1 into the 2MLN-dnTβRII cells, and these cells were injected into mice to form tumors. At day 7, the volume of 2MLN-dnTβRII tumors that expressed exogenous thrombospondin-1 (3.08×10^3 mm^3) was lower than that of 2MLN-dnTβRII tumors alone (12.0×10^3 mm^3) (difference = 8.94×10^3 mm^3, 95% CI = 5.82×10^3 to 12.1×10^3 mm^3, $P < .001$ [n = 6]) and was similar to that of control 2MLN-GFP tumors that expressed GFP (2.81×10^3 mm^3; difference = 0.27×10^3 mm^3, 95% CI = -1.67×10^3 to 2.21×10^3 mm^3, $P = .76$ [n = 6]) (Figure 4, A). Immunostaining of the tumors with an antibody against PECAM-1 protein demonstrated that the vascular density of the 2MLN-dnTβRII tumors was reduced by the introduction of thrombospondin-1 (1.90% per microscopic field) compared with that of 2MLN-dnTβRII tumors alone (7.74%; difference = 5.84%, 95% CI = 4.21% to 7.48%, $P < .001$ [n = 3]) or that of 2MLN-GFP tumors as control (1.85% per microscopic field; difference = 0.05%, 95% CI = −1.64% to 1.73%, $P = .9$ [n = 3]) (Figure 4, B). In contrast, AZAN staining showed that the degree of fibrosis was not statistically significantly changed by introduction of thrombospondin-1 (Figure 4, C).

We obtained additional support for the finding that decrease in thrombospondin-1 is involved in the accelerated growth of the 2MLN-dnTβRII tumors by knocking down the expression of thrombospondin-1 in the 2MLN-GFP cells with an RNA interference approach. The 2MLN-GFP cells expressing the microRNA construct against thrombospondin-1 were termed 2MLN-GFP+miTSP-1 cells. Expression of thrombospondin-1 was lower in the 2MLN-GFP+miTSP-1 cells than in 2MLN-GFP cells in vitro (Figure 4, D). When these cells were inoculated to mice to form tumors, knockdown of thrombospondin-1 resulted in the volumes of 2MLN-GFP+miTSP-1 tumors being larger than those of 2MLN-GFP tumors (Figure 4, E; mean volume of 2MLN-GFP+miTSP-1 tumor on day 14 relative to that on day 0 after starting evaluation = 4.91 and that of 2MLN-GFP tumor = 3.79; difference = 1.12, 95% CI = 0.80 to 1.44; for group effect, sampling time effect, and group effect × sampling time effect, $P < .001$, by a two-way repeated measures ANOVA test for tumor growth [n = 6 in each group]). In addition, 2MLN-GFP+miTSP-1 tumors were smaller than 2MLN-dnTβRII tumors (Figure 4, E; volume of 2MLN-GFP+miTSP-1 tumor on day 14 relative to that on day 0 after starting evaluation = 4.91 and that of 2MLN-dnTβRII tumor = 5.65; difference = 0.74, 95% CI = −0.78 to 2.27; the result of a two-way repeated measures ANOVA test for the tumor growth from days 0 to 14 [n = 6 in each group] for group effect, $P = .010$; for sampling time effect, $P < .001$; for group effect × sampling time effect, $P = .025$), in agreement with the finding that the in vivo expression level of thrombospondin-1 mRNA in the 2MLN-GFP+miTSP-1 tumors (0.42) was higher than that of the 2MLN-dnTβRII tumors (0.12; difference = 0.30, 95% CI = 0.12 to 0.49; $P = .011$) (Figure 4, F).

To further elucidate the contribution of enhanced angiogenesis to increased tumor growth in the gastric carcinoma model, we treated the tumor-bearing mice with sorafenib, a small-molecule inhibitor of various tyrosine kinases, including VEGF receptor-2, Raf, and platelet-derived growth factor receptor (30,31). Sorafenib (40 mg/kg) or a vehicle control was intraperitoneally administered into the tumor-bearing mice every day (n = 6 mice per group). Treatment with sorafenib strongly suppressed the growth of both 2MLN-GFP tumors (Figure 5, A; tumor volume in treated mice on day 14 relative to that on day 0 after starting evaluation = 0.45 and that in untreated mice = 2.73; difference = 2.28, 95% CI = 1.81 to 2.76; for group effect, sampling time effect, and group effect × sampling time effect, $P < .001$, by a two-way repeated measures ANOVA test for tumor growth) and 2MLN-dnTβRII tumors (Figure 5, A; tumor volume in treated mice on day 14 relative to that on day 0 after starting evaluation = 0.79 and that in untreated mice = 7.64; difference = 6.85, 95% CI = 4.34 to 9.37; for group effect, sampling time effect, and group effect × sampling time effect, $P < .001$, by a two-way repeated measures ANOVA test for tumor growth). The tumors treated with sorafenib were pale in comparison with the untreated tumors, indicating the reduction of tumor vasculature and thus hemoglobin. To further confirm the effects of inhibition of angiogenesis on the tumor growth, an anti-VEGF neutralizing antibody (2.5 mg/kg) or a vehicle control was intraperitoneally administered into the tumor-bearing mice twice a week (n = 8 mice per group). As with sorafenib treatment, treatment with the anti-VEGF neutralizing antibody reduced the volume of both 2MLN-GFP tumors (Figure 5, B; tumor volume in treated mice on day 14 relative to that on day 0 after starting evaluation = 1.89 and that in control treated mice = 3.72; difference = 1.83, 95% CI = 0.68 to 2.98; for group effect, $P = .003$; and for sampling time effect and group effect × sampling time effect, $P < .001$, by a two-way repeated measures ANOVA test for tumor growth) and 2MLN-dnTβRII

tumors (Figure 5, B; tumor volume in treated mice on day 14 relative to that on day 0 after starting evaluation = 1.90 and that in control treated mice = 8.05; difference = 6.15, 95% CI = 0.12 to 12.18; for group effect, $P = .011$; and for sampling time effect and group effect × sampling time effect, $P < .001$, by a two-way repeated measures ANOVA test for tumor growth).

Disruption of TGF-β Signaling in Another Diffuse-Type Gastric Carcinoma Cell Line

In addition to OCUM-2MLN cells, we also used another diffuse-type gastric carcinoma cell line, OCUM-12, to investigate the effects of disruption of TGF-β signaling. TGF-β induced phosphorylation of Smad2 (Supplementary Figure 2, A, available online) and inhibited the proliferation of OCUM-12 cells in vitro (Supplementary Figure 2, B, available online), indicating that this cell line also responds to TGF-β. To further examine the effects of disrupting TGF-β signaling in this cell line, we generated OCUM-12 cells expressing GFP or dnTβRII and used them to confirm that phosphorylation of Smad2 was attenuated in OCUM-12-dnTβRII cells (Supplementary Figure 2, A, available online). We found that TGF-β1–induced thrombospondin-1 expression was attenuated in the OCUM-12-dnTβRII cells as it was in 2MLN-dnTβRII cells (Figure 5, C). Moreover, the volume of the OCUM-12 tumors expressing dnTβRII was statistically significantly larger than that of OCUM-12-GFP tumors (Figure 5, D; volume of OCUM-12-dnTβRII tumor on day 14 relative to that on day 0 after starting evaluation = 2.19 and that of OCUM-12-GFP tumor = 1.80; difference = 0.39, 95% CI = 0.014 to 0.772; for group effect, $P = .046$; for sampling time effect, $P < .001$; for group effect × sampling time effect, $P = .003$, by a two-way repeated measures ANOVA test for tumor growth [n = 7 mice in each group]), and sorafenib reduced the volume of both OCUM-12-GFP tumors (volume of treated tumor on day 14 relative to that on day 0 after starting evaluation = 1.17 and that of untreated tumor = 1.80; difference = 0.63, 95% CI = 0.28 to 0.98; for group effect, $P = .001$; and for sampling time effect and group effect × sampling time effect, $P < .001$, by a two-way repeated measures ANOVA test for tumor growth [n = 7 mice in each group]) and OCUM-12-dnTβRII tumors (volume of treated tumor on day 14 relative to that on day 0 after starting evaluation = 1.36 and that of untreated tumor = 2.19; difference = 0.83, 95% CI = 0.51 to 1.15; for group effect, $P < .001$; for sampling time effect and group effect × sampling time effect, $P < .001$, by a two-way repeated measures ANOVA test for tumor growth [n = 7 mice in each group]).

Expression of Thrombospondin-1 and Phosphorylated Smad2 in Human Gastric Carcinoma Tissues

Finally, we examined the status of TGF-β signaling in human gastric tumor tissues by use of antibody against phosphorylated Smad2 and the level of expression of thrombospondin-1 with antibody against thrombospondin-1. Both phosphorylated Smad2 and thrombospondin-1 were detected in normal epithelium adjacent to tumor (data not shown) and in some diffuse- and intestinal-type gastric cancer tissues (Supplementary Figure 3, A, available online). Immunostaining of 102 human gastric cancer specimens revealed that 44 (43%) tumors expressed both phosphorylated Smad2 and thrombospondin-1 and that 24 (23%) expressed neither (Supplementary Table 3, available online). Furthermore, a positive association was observed between the expression of thrombospondin-1 and of phosphorylated Smad2 ($P = .002$; Supplementary Table 3, available online). We also found that some cancer cells had weaker staining of phosphorylated Smad2 associated with weaker staining of thrombospondin-1 and that these cells were adjacent to cancer cells with strongly positive staining of phosphorylated Smad2 and strongly positive thrombospondin-1 (Supplementary Figure 3, B, available online). This observation suggested that the level of expression of thrombospondin-1 may be associated with the level of TGF-β signaling in each cancer cell, which varied even in the same tumor tissue.

Discussion

We demonstrated in this study that disruption of TGF-β signaling in diffuse-type gastric carcinoma models appears to accelerate the progression of cancer, as shown by increased growth of the 2MLN-dnTβRII tumors compared with that of the control 2MLN-GFP tumors in the subcutaneous and orthotopic transplantation models. Furthermore, microarray analysis of gene expression revealed decreased production of thrombospondin-1 in the 2MLN-dnTβRII tumors. Overexpression of thrombospondin-1 suppressed the growth of OCUM-2MLN tumors, but knockdown of thrombospondin-1 expression stimulated tumor growth. Moreover, we have also demonstrated that regulation of angiogenesis by sorafenib or anti-VEGF antibody efficiently prevented the growth of tumors in vivo.

Systemic administration of TGF-β inhibitors has been shown to suppress growth and metastasis of some tumors by acting on cancer cells and the tumor microenvironment (32,33). However, we found that disruption of TGF-β signaling in diffuse-type gastric carcinoma cells accelerated tumor formation. We found, in experiments with a mixture of the wild-type OCUM-2MLN cells and OCUM-2MLN cells expressing dnTβRII, that the increased growth of 2MLN-dnTβRII tumors appeared to be mainly attributable to alterations in the tumor microenvironment, not to autonomous properties of the cancer cells. The tumor microenvironment, which has been reported to be important during tumor progression (6), contains many structural elements, including blood vessels and fibrotic tissues. Consistently, we found that absence of TGF-β–induced expression of thrombospondin-1, an angiogenic inhibitor, is associated with increased growth of dnTβRII tumors in vivo, indicating that increased angiogenesis in the dnTβRII-expressing tumors appears to be important in the accelerated growth of such tumors.

TGF-β binds to TβRII and TGF-β type I receptorand activates Smad2 and Smad3, which transduce signals by complexing with Smad4. Decreased expression of TβRII, Smad2, and Smad4, or loss-of-function mutations in at least one of these genes, has been reported in various cancers at advanced stages, including breast cancer and colon cancer (16). Decreased expression of Smad4 has been observed in many clinical specimens of diffuse-type gastric carcinoma (20,34). Although mutations in TβRII have not been reported in diffuse-type gastric carcinoma, these findings indicate that disruption of TGF-β signaling may accelerate the progression of this type of cancer at advanced stages.

Schwarte-Waldhoff et al. (29) reported that the lack of Smad4 in an experimental pancreatic cancer model stimulated secretion of VEGF, repressed the expression of thrombospondin-1, and led to increased angiogenesis and tumor growth. Our microarray data revealed that although expression of VEGF was not statistically significantly altered in the 2MLN-dnTβRII tumors, compared with the 2MLN-GFP tumors, expression of thrombospondin-1 was reduced. Moreover, we found that the expression of thrombospondin-1 was induced by TGF-β in the OCUM-2MLN cells but not in the 2MLN-dnTβRII cells, in agreement with previous reports on the induction of thrombospondin-1 by TGF-β in certain cell types, including hepatic HuH-7 cells, osteosarcoma MG63 cells, and rat tubular epithelial cells (35,36). We obtained similar results with another diffuse-type gastric carcinoma cell line, OCUM-12. Furthermore, we found that expression of thrombospondin-1 reduced the growth of 2MLN-dnTβRII tumors in mice and that growth of tumors produced from 2MLN-GFP cells in which thrombospondin-1 expression had been inhibited was accelerated. Moreover, the association that we found between the expression of phosphorylated Smad2 and thrombospondin-1 indicated that attenuation or loss of TGF-β signaling results in decreased expression of thrombospondin-1 in human gastric cancer tissues. Thrombospondin-1 has been shown to inhibit growth and differentiation of endothelial cells and to induce their apoptosis (24,25). Thus, the decreased level of thrombospondin-1 in these tumor models appears to accelerate tumor angiogenesis.

The importance of tumor angiogenesis in the accelerated growth of the 2MLN-dnTβRII tumors was further supported by the potent inhibition of tumor growth by treatment with sorafenib, regardless of the status of TGF-β signaling in the cancer cells. Sorafenib was effective not only in OCUM-2MLN tumors but also in OCUM-12 tumors, although the latter were relatively resistant to sorafenib's growth inhibitory effect in vitro (A. Komuro, M. R. Kano and K. Miyazono, University of Tokyo, M. Yashiro and K. Hirakawa, Osaka City University, unpublished data; the 50% inhibitory concentration [IC_{50}] in OCUM-2MLN cells = 1.45 μM and in OCUM-12 cells = 8.75 μM). Thus, the effect of sorafenib on the gastric tumor models in vivo may be mostly due to suppression of tumor angiogenesis, although direct effects of sorafenib on the gastric carcinoma cells may also contribute to its growth inhibitory effect in vivo. In accordance with these results, we found that an anti-VEGF neutralizing antibody effectively reduced the growth of OCUM-2MLN tumors.

Our study had several limitations. Although we examined the growth of diffuse-type gastric carcinoma in subcutaneous and orthotopic transplantation models, the experiments were conducted with immunocompromised mice. Immune function may affect the growth of diffuse-type gastric carcinoma in human patients. Furthermore, we analyzed the growth of primary tumors but not the metastasis of tumors. The question of whether TGF-β signaling regulates metastasis in a cancer cell–autonomous fashion or in a microenvironment-dependent manner should be explored in the future.

In conclusion, we have shown that disruption of TGF-β signaling in a mouse model of diffuse-type gastric carcinoma, which may be analogous to what occurs during progression of this disease in humans, promotes tumorigenesis by accelerating angiogenesis. Because the loss of TβRII or Smad4 expression has been reported to induce tumor angiogenesis in other types of cancers (29,37), the administration of angiogenesis inhibitors, including sorafenib and thrombospondin-1 analogues (38), may be useful as a treatment for those cancers with disrupted TGF-β signaling pathways.

References

1. Crew KD, Neugut AI. Epidemiology of gastric cancer. *World J Gastroenterol.* 2006;12(3):354–362.
2. Hohenberger P, Gretschel S. Gastric cancer. *Lancet.* 2003;362(9380):305–315.
3. Laurén P. The two histological main types of gastric carcinoma: diffuse and so-called intestinal-type carcinoma. *Acta Pathol Microbiol Scand.* 1965;64:31–49.
4. Yashiro M, Chung YS, Nishimura S, Inoue T, Sowa M. Establishment of two new scirrhous gastric cancer cell lines: analysis of factors associated with disseminated metastasis. *Br J Cancer.* 1995;72(5):1200–1210.
5. Henson DE, Dittus C, Younes M, Nguyen H, Albores-Saavedra J. Differential trends in the intestinal and diffuse types of gastric carcinoma in the United States, 1973–2000. *Arch Pathol Lab Med.* 2004;128(7):765–770.
6. Bierie B, Moses HL. TGF-β and the tumor microenvironment. In: Derynck R, Miyazono K, eds. *The TGF-β Family.* New York, NY: Cold Spring Harbor Laboratory Press; 2008:965–987.
7. Feng XH, Derynck R. Specificity and versatility in TGF-β signaling through Smads. *Annu Rev Cell Dev Biol.* 2005;21:659–693.
8. Shi Y, Massagué J. Mechanisms of TGF-β signaling from cell membrane to the nucleus. *Cell.* 2003;113(6):685–700.
9. Roberts AB, Wakefield LM. The two faces of transforming growth factor β in carcinogenesis. *Proc Natl Acad Sci USA.* 2003;100(15):8621–8623.
10. Moustakas A, Heldin CH. Signaling networks guiding epithelial-mesenchymal transitions during embryogenesis and cancer progression. *Cancer Sci.* 2007;98(10):1512–1520.
11. Akhurst RJ. TGF-β signaling in epithelial-mesenchymal transition and invasion and metastasis. In: Derynck R, Miyazono K, eds. *The TGF-β Family.* New York, NY: Cold Spring Harbor Laboratory Press; 2008:939–964.
12. Yin JJ, Selander K, Chirgwin JM, et al. TGF-β signaling blockade inhibits PTHrP secretion by breast cancer cells and bone metastases development. *J Clin Invest.* 1999;103(2):197–206.
13. Muraoka RS, Dumont N, Ritter CA, et al. Blockade of TGF-β inhibits mammary tumor cell viability, migration, and metastases. *J Clin Invest.* 2002;109(12):1551–1559.
14. Yang YA, Dukhanina O, Tang B, et al. Lifetime exposure to a soluble TGF-β antagonist protects mice against metastasis without adverse side effects. *J Clin Invest.* 2002;109(12):1607–1615.
15. Azuma H, Ehata S, Miyazaki H, et al. Effect of Smad7 expression on metastasis of mouse mammary carcinoma JygMC(A) cells. *J Natl Cancer Inst.* 2005;97(23):1734–1746.
16. Lahn M, Berry B, Kloeker S, Yingling JM. TGF-β receptor kinase inhibitors for the treatment of cancer. In: ten Dijke P, Heldin CH, eds. *Smad Signal Transduction.* New York, NY: Springer Verlag; 2006:415–442.
17. Mizoi T, Ohtani H, Miyazono K, et al. Immunoelectron microscopic localization of transforming growth factor β1 and latent transforming growth factor β1 binding protein in human gastrointestinal carcinomas: qualitative difference between cancer cells and stromal cells. *Cancer Res.* 1993;53(1):183–190.
18. Kinugasa S, Abe S, Tachibana M, et al. Overexpression of transforming growth factor-β1 in scirrhous carcinoma of the stomach correlates with decreased survival. *Oncology.* 1998;55(6):582–587.
19. Vagenas K, Spyropoulos C, Gavala V, Tsamandas AC. TGFβ1, TGFβ2, and TGFβ3 protein expression in gastric carcinomas: correlation with prognostics factors and patient survival. *J Surg Res.* 2007;139(2):182–188.
20. Kim JY, Park DY, Kim GH, et al. Smad4 expression in gastric adenoma and adenocarcinoma: frequent loss of expression in diffuse type of gastric adenocarcinoma. *Histol Histopathol.* 2005;20(2):543–549.
21. Fujihara T, Sawada T, Hirakawa K, et al. Establishment of lymph node metastatic model for human gastric cancer in nude mice and analysis of factors associated with metastasis. *Clin Exp Metastasis.* 1998;16(4):389–398.

22. Qiu H, Yashiro M, Shinto O, Matsuzaki T, Hirakawa K. DNA methyltransferase inhibitor 5-aza-CdR enhances the radiosensitivity of gastric cancer cells. *Cancer Sci.* 2009;100(1):181–188.
23. Shibuya K, Shirakawa J, Kameyama T, et al. CD226 (DNAM-1) is involved in lymphocyte function-associated antigen 1 costimulatory signal for naive T cell differentiation and proliferation. *J Exp Med.* 2003;198(12):1829–1839.
24. Yamauchi M, Imajoh-Ohmi S, Shibuya M. Novel antiangiogenic pathway of thrombospondin-1 mediated by suppression of the cell cycle. *Cancer Sci.* 2007;98(9):1491–1497.
25. Jiménez B, Volpert OV, Crawford SE, Febbraio M, Silverstein RL, Bouck N. Signals leading to apoptosis-dependent inhibition of neovascularization by thrombospondin-1. *Nat Med.* 2000;6(1):41–48.
26. Dennis G Jr, Sherman BT, Hosack DA, et al. DAVID: Database for Annotation, Visualization, and Integrated Discovery. *Genome Biol.* 2003;4(5):P3.
27. Zhang J, Ito R, Oue N, et al. Expression of thrombospondin-1 is correlated with microvessel density in gastric carcinoma. *Virchows Archiv.* 2004;442(6):563–568.
28. Eguchi T, Inoue T, Fujii K, et al. Laminin-5 (gamma2 chain) is a marker of invading cancer cells in human gallbladder carcinoma: special emphasis on extension of carcinoma in situ along Rokitansky-Aschoff sinuses. *Oncol Rep.* 2008;20(1):33–39.
29. Schwarte-Waldhoff I, Volpert OV, Bouck NP, et al. Smad4/DPC4-mediated tumor suppression through suppression of angiogenesis. *Proc Natl Acad Sci USA.* 2000;97(17):9624–9629.
30. Wilhelm S, Carter C, Lynch M, et al. Discovery and development of sorafenib: a multikinase inhibitor for treating cancer. *Nat Rev Drug Discov.* 2006;5(10):835–844.
31. Liu L, Cao Y, Chen C, et al. Sorafenib blocks the RAF/MEK/ERK pathway, inhibits tumor angiogenesis, and induces tumor cell apoptosis in hepatocellular carcinoma model PLC/PRF/5. *Cancer Res.* 2006;66(24):11851–11858.
32. Nam JS, Terabe M, Mamura M, et al. An anti-transforming growth factor β antibody suppresses metastasis via cooperative effects on multiple cell compartments. *Cancer Res.* 2008;68(10):3835–3843.
33. Kawajiri H, Yashiro M, Shinto O, et al. A novel transforming growth factor β receptor kinase inhibitor, A-77, prevents the peritoneal dissemination of scirrhous gastric carcinoma. *Clin Cancer Res.* 2008;14(9):2850–2860.
34. Okano H, Shinohara H, Miyamoto A, Takaori K, Tanigawa N. Concomitant overexpression of cyclooxygenase-2 in HER-2-positive on Smad4-reduced human gastric carcinomas is associated with a poor patient outcome. *Clin Cancer Res.* 2004;10(20):6938–6945.
35. Okamoto M, Ono M, Uchiumi T, et al. Up-regulation of thrombospondin-1 gene by epidermal growth factor and transforming growth factor β in human cancer cells—transcriptional activation and messenger RNA stabilization. *Biochim Biophys Acta.* 2002;1574(1):24–34.
36. Nakagawa T, Lan HY, Glushakova O, et al. Role of ERK1/2 and p38 mitogen-activated protein kinases in the regulation of thrombospondin-1 by TGF-β1 in rat proximal tubular cells and mouse fibroblasts. *J Am Soc Nephrol.* 2005;16(4):899–904.
37. Lu SL, Herrington H, Reh D, et al. Loss of transforming growth factor-β type II receptor promotes metastatic head-and-neck squamous cell carcinoma. *Genes Dev.* 2006;20(10):1331–1342.
38. Ebbinghaus S, Hussain M, Tannir N, et al. Phase 2 study of ABT-510 in patients with previously untreated advanced renal cell carcinoma. *Clin Cancer Res.* 2007;13(22 Pt 1):6689–6695.

Funding

KAKENHI (Grant-in-Aid for Scientific Research; Project No. 17016011) from the Ministry of Education, Culture, Sports, Science, and Technology of Japan.

Notes

The study sponsors had no role in the design of the study or in the collection, analysis, or interpretation of the data. The authors take full responsibility for the study design, data collection, analysis and interpretation of the data, the decision to submit the manuscript for publication, and the writing of the manuscript.
We are grateful to Masako Oka for discussion, and Hiroko Yanagisawa, Makoto Arai, Saori Sakaue, and Satoru Yonekura for technical assistance.

Manuscript received August 6, 2008; revised January 28, 2009; accepted February 20, 2009.

Autophagy Is Activated by TGF-β and Potentiates TGF-β–Mediated Growth Inhibition in Human Hepatocellular Carcinoma Cells

Kunihiko Kiyono,[1] Hiroshi I. Suzuki,[1] Hironori Matsuyama,[1] Yasuyuki Morishita,[1] Akiyoshi Komuro,[1] Mitsunobu R. Kano,[1] Koichi Sugimoto,[2] and Kohei Miyazono[1]

[1]Department of Molecular Pathology, Graduate School of Medicine, University of Tokyo and [2]Division of Hematology, Department of Internal Medicine, Juntendo University School of Medicine, Tokyo, Japan

Abstract

Transforming growth factor-β (TGF-β) is a multifunctional cytokine that regulates cell growth, differentiation, and apoptosis of various types of cells. Autophagy is emerging as a critical response of normal and cancer cells to environmental changes, but the relationship between TGF-β signaling and autophagy has been poorly understood. Here, we showed that TGF-β activates autophagy in human hepatocellular carcinoma cell lines. TGF-β induced accumulation of autophagosomes and conversion of microtubule-associated protein 1 light chain 3 and enhanced the degradation rate of long-lived proteins. TGF-β increased the mRNA expression levels of BECLIN1, ATG5, ATG7, and death-associated protein kinase (DAPK). Knockdown of Smad2/3, Smad4, or DAPK, or inhibition of c-Jun NH_2-terminal kinase, attenuated TGF-β–induced autophagy, indicating the involvement of both Smad and non-Smad pathway(s). TGF-β activated autophagy earlier than execution of apoptosis (6-12 versus 48 h), and reduction of autophagy genes by small interfering RNA attenuated TGF-β–mediated growth inhibition and induction of proapoptotic genes Bim and Bmf, suggesting the contribution of autophagy pathway to the growth-inhibitory effect of TGF-β. Additionally, TGF-β also induced autophagy in some mammary carcinoma cells, including MDA-MB-231 cells. These findings show that TGF-β signaling pathway activates autophagy in certain human cancer cells and that induction of autophagy is a novel aspect of biological functions of TGF-β. [Cancer Res 2009;69(23):8844–52]

Introduction

Autophagy is an evolutionally conserved lysosomal degradation pathway in which the cell self-digests its proteins and organelles and thus maintains macromolecular synthesis and ATP production (1). Autophagy enables the cell to survive under various stress conditions including nutrient deprivation, growth factor depletion, and hypoxia (2–5). Moreover, autophagy plays an important role in the elimination of misfolded protein aggregates, invading microorganisms, and damaged organelles (6, 7).

During autophagy, the isolation membrane is initially formed. The membrane wraps some cytoplasmic contents and transforms into the autophagosome, which then fuses with the lysosome and degrades its contents (2, 8, 9). Autophagy-related gene (ATG) products play essential roles in autophagy. Autophagosome formation is mediated by two ubiquitin-like conjugation systems composed of ATG proteins, which culminate in conjugation of ATG12 to ATG5 and conversion of a soluble form of microtubule-associated protein 1 light chain 3 (LC3-I) to phosphatidylethanolamine-conjugated membrane-bound form (LC3-II; refs. 1, 9). BECLIN1 is a component of the class III phosphoinositide 3-kinase complex and also plays an important role in autophagy regulation. Depletion of cellular energy and reduced amino acid levels stimulate autophagy through the inhibition of mammalian target of rapamycin (mTOR; 1, 9).

Although autophagy might allow tumor cells to survive under metabolic stress (10), several genetic links have emerged between defects of autophagy and development of cancer. *BECLIN1* is monoallelically deleted in 40% to 75% of human breast, ovarian, and prostate cancers and thus considered as a tumor suppressor gene (11, 12). Accordingly, heterozygous deletion of *BECLIN1* in mice resulted in increased incidence of spontaneous tumors (13). Moreover, autophagy and apoptosis might be linked to each other and occur simultaneously or sequentially in a cell type–, death stimulus–, and context-dependent manner (5). In this context, several studies describe a role for autophagy in antagonizing cell survival and promoting cell death (4, 14). Furthermore, loss of *BECLIN1* or *ATG5* may promote genomic instability, which might ultimately lead to progression of tumors (10, 15).

Transforming growth factor-β (TGF-β) regulates the growth, differentiation, and migration of various types of cells. Similar to the duality of autophagy in oncogenesis, TGF-β functions as both tumor suppressor and tumor promoter (16, 17). In early stages of carcinogenesis, TGF-β serves as a tumor suppressor through inhibition of cell growth. However, some tumor cells escape from the growth inhibition by TGF-β, and TGF-β facilitates the progression and metastasis of tumors in advanced cancer.

TGF-β has been reported to induce autophagy in normal bovine mammary epithelial BME-UV1 cells (18). However, mechanisms for activation of autophagy by TGF-β and its role in growth of cancer cells have not been elucidated. In the present study, we showed that TGF-β activates autophagy in hepatocellular carcinoma cells and mammary carcinoma cells.

Materials and Methods

Cell lines. HuH7 cells were from Health Science Research Resources Bank. MDA-MB-231 cells were from the American Type Culture Collection.

Antibodies and reagents. The antibodies used were as follows: anti-LC3 (nanoTools) or PM036 (MBL), anti-BECLIN1 (BD Biosciences), anti-ATG5 (Cosmo Bio Co), anti-ATG7 (MBL), anti–death-associated protein kinase (DAPK; BD Biosciences), anti–poly(ADP-ribose) polymerase (Cell

---

Note: Supplementary data for this article are available at Cancer Research Online (http://cancerres.aacrjournals.org/).

K. Kiyono and H.I. Suzuki contributed equally to this work.

Requests for reprints: Kohei Miyazono, Department of Molecular Pathology, Graduate School of Medicine, University of Tokyo, 7-3-1 Hongo, Bunkyo-ku, Tokyo 113-0033, Japan. Phone: 81-3-5841-3345; Fax: 81-3-5841-3354; E-mail: miyazono@m.u-tokyo.ac.jp.

doi:10.1158/0008-5472.CAN-08-4401

Signaling), and anti–α-tubulin (Sigma). The reagents used were as follows: TGF-β1 (R&D Systems), LY364947 (Calbiochem), SB431542 (Sigma-Aldrich), mitogen-activated protein kinase (MAPK) inhibitors (Calbiochem), 3-methyladenine (3-MA; Sigma-Aldrich), and bafilomycin A1 (BafA1; Wako).

Small interfering RNA and oligonucleotides. Small interfering RNAs (siRNA) were introduced with 20 nmol/L using HiPerfect reagent (Qiagen). The transfected cells were used for subsequent experiments after 24 to 48 h. The details of siRNAs are given in Supplementary Table S1. Knockdown efficacies were shown in Supplementary Figures.

Lentiviral-mediated transfer. GFP-LC3 cDNA (19) and kinase-inactive form of TβRI were transferred into lentiviral vector (CSII-CMV-RfA) and introduced by lentiviral infection system (20).

Fluorescence and electron microscopy. Cells were observed by a fluorescence microscope (Olympus IX70). The sequential change of the LC3 localization was examined using Leica DMR fluorescence microscope (Leica Microsystems). The percentage of cells with more than four GFP-LC3 dots was quantified according to the previous report (21). The areas of LC3 dots were analyzed using ImageJ software (NIH). Transmission electron microscopy was done using JEOL 1200EX electron microscope as described previously (22).

Immunoblotting. Cultured cells were lysed in a buffer containing 50 mmol/L Tris-HCl (pH 8.0), 150 mmol/L NaCl, phosphatase inhibitors, 1% Triton X-100, and 1% protease inhibitor cocktail (Nacalai Tesque). Detailed procedures of immunoblotting were described previously (23).

Long-lived protein degradation. Degradation rates of long-lived proteins were determined as reported previously (24, 25).

RNA isolation and quantitative reverse transcription-PCR. Total RNAs were extracted using RNeasy Mini kit (Qiagen). First-strand cDNAs were synthesized using the Quantitect Reverse Transcription kit (Qiagen). Quantitative reverse transcription-PCR analysis was done by the absolute standard curve method using the 7500 Fast Real-time PCR System (Applied Biosystems). Values were normalized to human HPRT1. The primer sequences used are given in Supplementary Table S2.

Growth inhibition assay, apoptosis assay, and cell cycle analysis. Cells (3×10^3) were seeded in 96-well plates and transfected with siRNAs. After TGF-β treatment, cell viability was quantified by colorimetric assay using WST-8 (Nacalai Tesque). Apoptosis was assessed by terminal deoxynucleotidyl transferase-mediated dUTP nick end labeling assay (APO-DIRECT kit; BD Biosciences) and Hoechst 33342 staining (Sigma). Cell cycle profiling was done using the CycleTEST PLUS DNA Reagent kit (BD Biosciences).

Results

TGF-β induces autophagy in human hepatocellular carcinoma cell lines. Mechanisms of TGF-β–mediated growth inhibition have been well investigated, particularly in hepatocytes, certain epithelial cells, and lymphocytes (26). Because many lines of evidence suggest a link between autophagy and cell death including apoptosis (5), we first examined the effect of TGF-β on autophagy in HuH7 human hepatocellular carcinoma cells, which undergo apoptosis and cell cycle arrest by TGF-β (27). Analysis of GFP-LC3 localization is widely used for monitoring autophagy (19). Because transiently overexpressed LC3 tends to aggregate in an autophagy-independent manner (28), we generated HuH7 cells stably expressing GFP-LC3 by lentiviral infection system. Relocalization of GFP-LC3 to the autophagosomes was detected as dot formation. Treatment with 1 ng/mL TGF-β for 12 to 24 h induced GFP-LC3 dot formation in HuH7 cells (Fig. 1*A*). Transmission electron microscopy showed the formation of autophagosomes after TGF-β

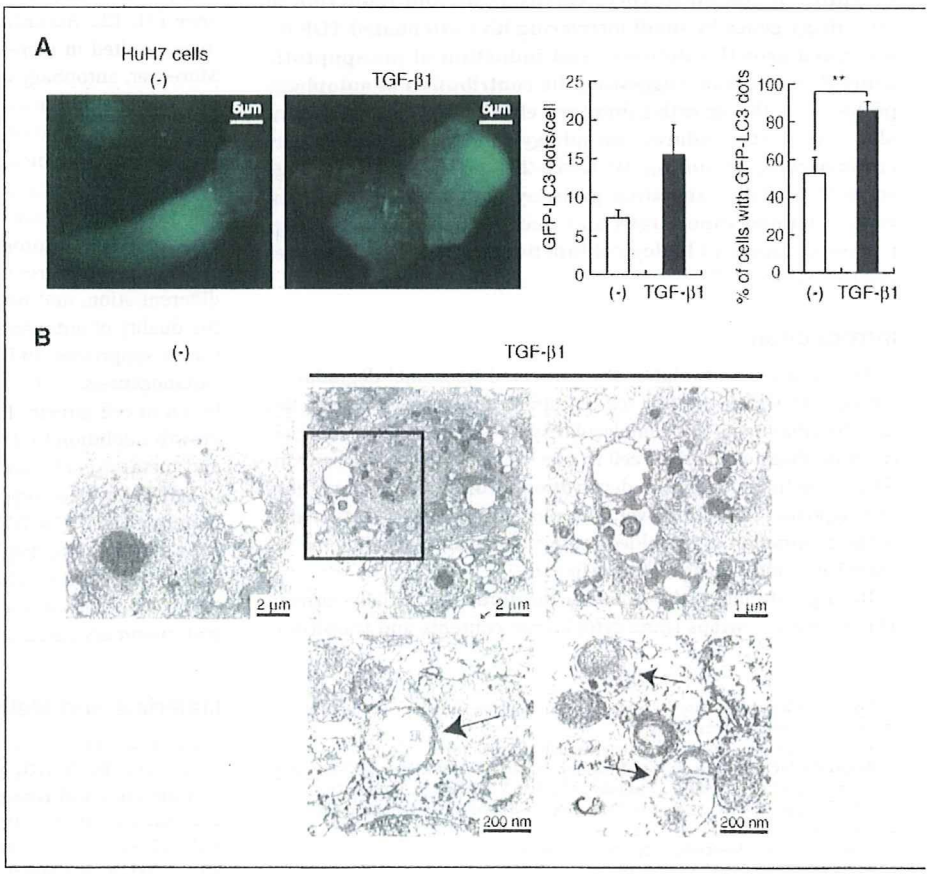

Figure 1. Autophagosome formation is stimulated by TGF-β in HuH7 hepatocellular carcinoma cells. *A*, HuH7 stably expressing GFP-LC3 were treated with 1 ng/mL TGF-β1 for 24 h. GFP-LC3 dot formation was observed by phase-contrast microscopy (*left*). The number of GFP-LC3 dots per cell and percentage of cells with more than four GFP-LC3 dots were quantified (*right*). *Columns*, mean of 20 cell counts (done in triplicate); *bars*, SE. **, $P < 0.01$. *B*, transmission electron microscopy showed formation of autophagosomes after TGF-β1 treatment (1 ng/mL, 24 h) in HuH7 cells. *Top right*, enlarged image of the box in the middle. Representative images of autophagosomes are shown at bottom (*arrows*).

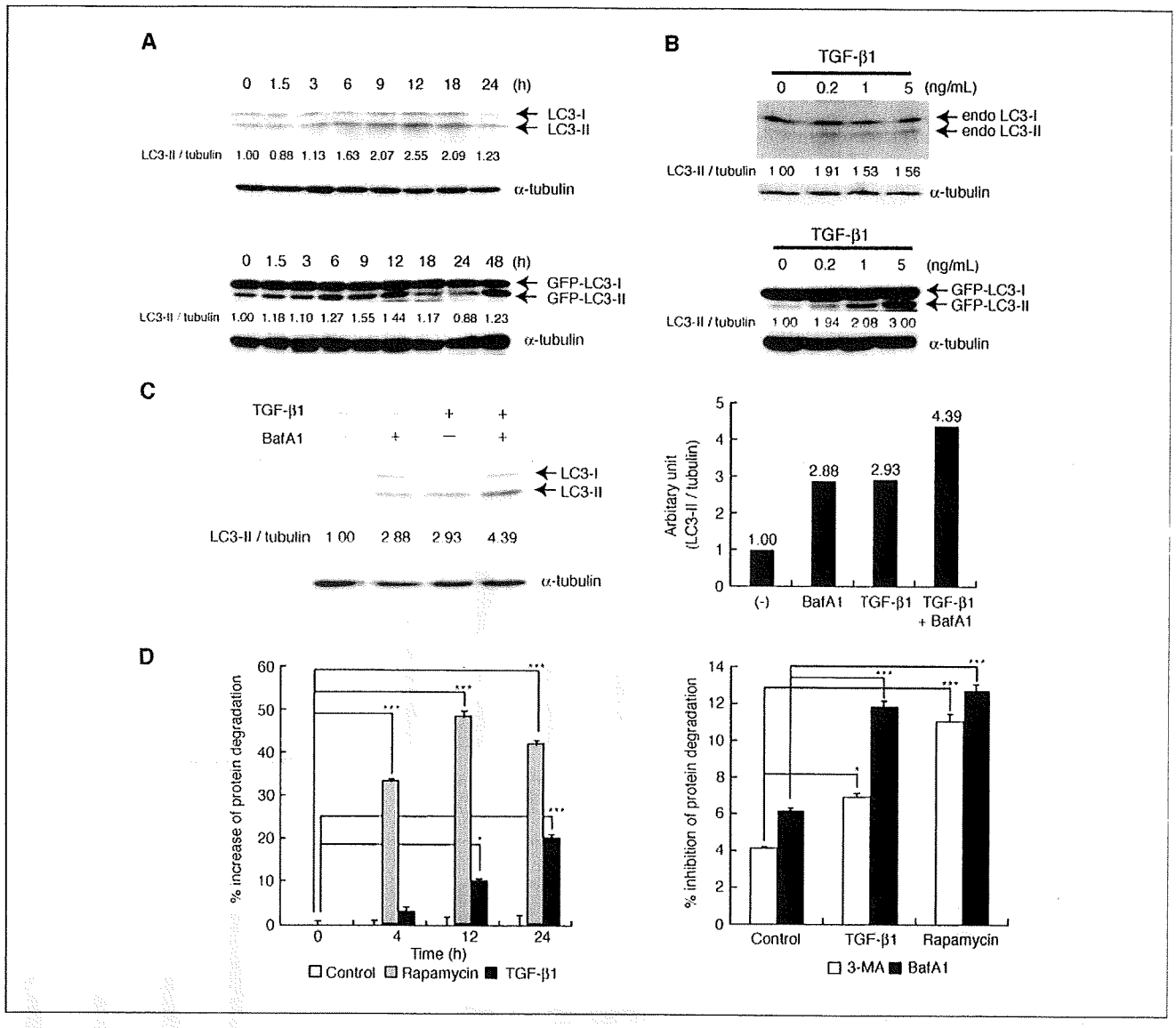

Figure 2. TGF-β stimulates LC3 conversion and long-lived protein degradation. *A*, immunoblot analysis of conversion of endogenous LC3 (*top*) and GFP-LC3 (*bottom*; LC3-I to LC3-II) in HuH7 cells by treatment with TGF-β1 (1 ng/mL). The LC3-II/tubulin ratio was calculated with ImageJ 1.36b. *B*, dose-dependent effect of TGF-β1 treatment (12 h) on endogenous LC3 (*top*) and GFP-LC3 (*bottom*) conversion. *C*, LC3 turnover assay. HuH7 cells were treated with TGF-β1 (1 ng/mL) for 12 h. The amount of endogenous LC3 was analyzed after 2 h treatment with or without BafA1 (20 nmol/L; *left*). The LC3-II/tubulin ratio is shown (*right*). *D*, rates of long-lived protein degradation were measured in HuH7 cells treated with TGF-β1 (1 ng/mL) or rapamycin (20 nmol/L) for indicated periods (*left*). The percentages of change were expressed by dividing the rate of degradation in TGF-β1– or rapamycin-treated cells by that in untreated cells. Effects of 3-MA or BafA1 on TGF-β–mediated enhancement of long-lived protein degradation were also determined (*right*). HuH7 cells were incubated with 3-MA (10 mmol/L) or BafA1 (10 nmol/L) during the treatment with TGF-β1 or rapamycin for 24 h. The percentages of change were expressed by subtracting the rate of degradation in 3-MA– or BafA1-treated cells from that in cells not treated with 3-MA or BafA1. *Columns*, mean of triplicate determinations; *bars*, SD. *, $P < 0.05$; ***, $P < 0.001$.

treatment (Fig. 1*B*). Autophagosomes were recognized as characteristic double-membrane vacuolar structures containing various kinds of cytoplasmic contents (Fig. 1*B*, *bottom*).

We next examined the induction of autophagy by immunoblot analysis for LC3, because LC3-II can be distinguished from LC3-I by the increased mobility of LC3-II. TGF-β converted endogenous and GFP-tagged LC3-I to LC3-II in HuH7 cells (Fig. 2*A*). Endogenous LC3-II increased between 6 and 12 h of TGF-β treatment. The amount of LC3-II gradually declined ~24 h of the treatment, suggesting that the autophagic process may degrade LC3-II (Fig. 2*A*, *top*). In contrast, GFP-tagged LC3-II increased biphasically (Fig. 2*A*, *bottom*). TGF-β also induced GFP-LC3 conversion in another human hepatoma cell line, HepG2 (Supplementary Fig. S1). GFP-LC3 conversion and dot formation depended on TGF-β concentration in the range of 0.2 to 5 ng/mL (Fig. 2*B*, *bottom*; Supplementary Fig. S2), although this dose dependency was not so apparent in case of endogenous LC3-II (Fig. 2*B*, *top*).

We next determined the autophagy flux by LC3 turnover assay, which measures the amount of LC3-II delivered to the lysosomes by comparing the LC3-II amounts in the presence and absence of lysosomal inhibitors (29, 30). Blockade of the autophagosome-lysosome fusion by a vacuolar H^+ ATPase inhibitor, BafA1, significantly increased accumulation of endogenous LC3-II, and TGF-β apparently augmented the BafA1-mediated LC3-II accumulation

(Fig. 2*C*). This cooperative effect with lysosomal inhibitor supports the hypothesis that TGF-β enhances autophagy flux *per se*.

Long-lived protein degradation assay is another well-established method for measuring autophagy flux (31, 32). TGF-β gradually enhanced degradation of long-lived proteins in HuH7 cells, although its effect was less potent and slower than rapamycin, a representative inhibitor of mTOR (Fig. 2*D, left*). Both 3-MA, an autophagy inhibitor, and BafA1 attenuated TGF-β–enhanced long-lived protein degradation (Fig. 2*D, right*). These results suggest that TGF-β enhances long-lived protein degradation through the activation of macroautophagy in the hepatoma cells.

Inhibition of ATG genes suppresses TGF-β–induced autophagy activation. We next explored whether TGF-β modulates the expression levels of ATG genes in HuH7 cells. Quantitative reverse transcription-PCR showed that treatment with 1 ng/mL TGF-β for 24 h significantly increased the expression levels of *BECLIN1*, *ATG5*, and *ATG7* (Fig. 3*A, left*). TGF-β also increased the mRNA level of *DAPK*, which stimulates autophagy and apoptosis (33, 34). Immunoblot analysis revealed that protein levels of ATG5 and DAPK were increased by TGF-β, whereas those of BECLIN1 and ATG7 did not apparently increase (Fig. 3*A, right*). We examined whether these ATG proteins regulate LC3 conversion by TGF-β. Downregulation of BECLIN1, ATG5 or ATG7 by siRNA inhibited TGF-β–stimulated LC3 conversion and GFP-LC3 dot formation in HuH7 cells (Fig. 3*B*; Supplementary Fig. S3). Temporal analysis also showed that ATG5 or ATG7 knockdown suppressed the biphasic increase of LC3-II by TGF-β (Fig. 3*C*).

Autophagy induction by TGF-β is mediated by TGF-β receptors, the Smad pathway, and c-Jun NH_2-terminal kinase. We then studied signaling pathways mediating autophagy induction by TGF-β. TGF-β binds to type I (TβRI) and type II (TβRII) receptors and transduces signals through receptor-regulated Smads (Smad2 and Smad3) and common-partner Smad (Smad4). Whereas TβRI triggers the Smad pathway, TβRII directly activates several

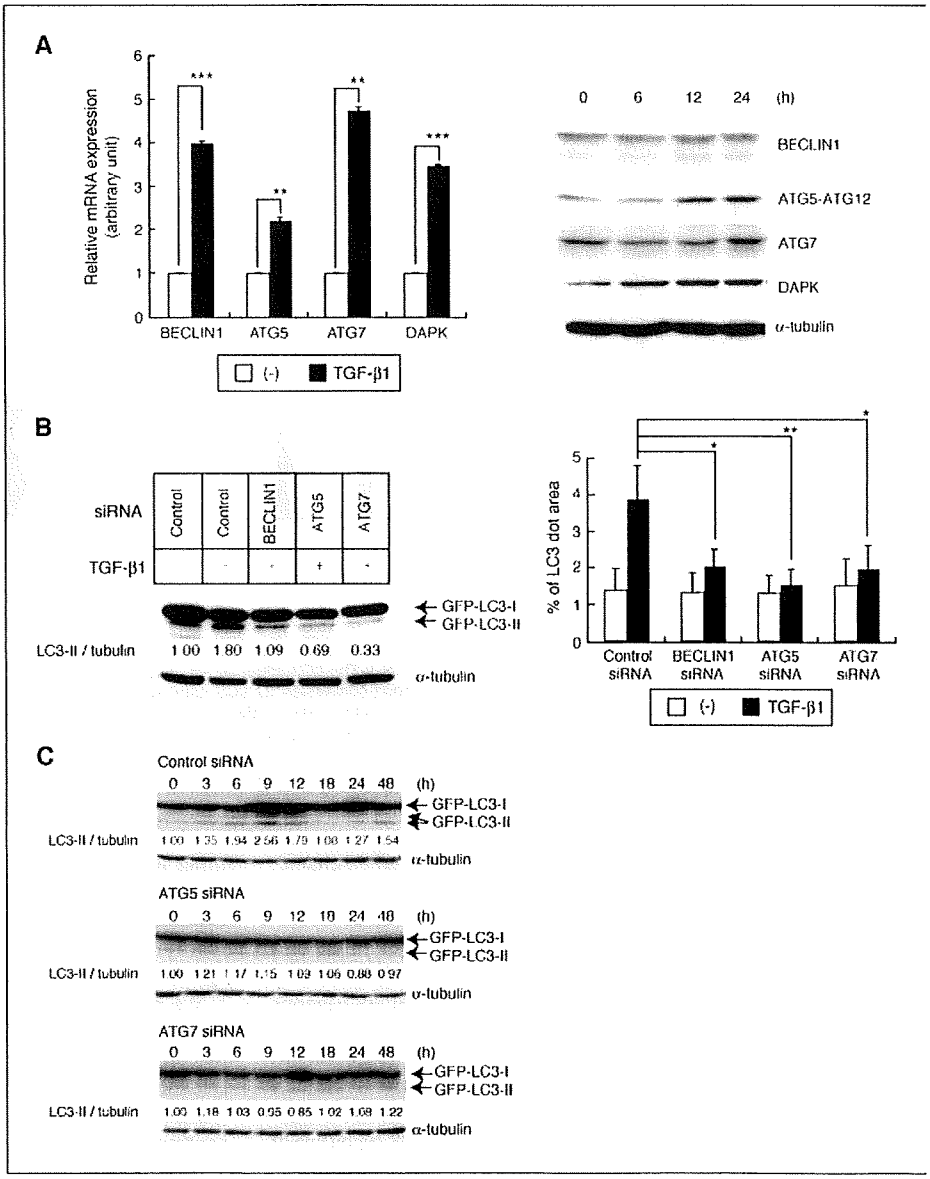

Figure 3. Effect of TGF-β on expression levels of ATG genes and their role in TGF-β–mediated autophagy activation. *A*, expression levels of autophagy-related genes (*BECLIN1, ATG5, ATG7*, and *DAPK*) in HuH7 cells. Quantitative reverse transcription-PCR analysis (*left*) and immunoblot analysis (*right*) were done after 24 h and indicated periods of TGF-β1 treatment (1 ng/mL), respectively. *Columns*, mean of triplicate determinations; *bars*, SD. **, $P < 0.01$; ***, $P < 0.001$. *B*, effects of BECLIN1, ATG5, or ATG7 knockdown on GFP-LC3 kinetics in HuH7 cells. Following siRNA transfection, GFP-LC3 conversion (*left*) and GFP-LC3 dot formation (*right*) were analyzed after 24 and 12 h of treatment with TGF-β1, respectively. *, $P < 0.05$; **, $P < 0.01$. *C*, effects of ATG5 or ATG7 knockdown by siRNA transfection on temporal change of GFP-LC3 by TGF-β.

other responses (35). Dominant-negative mutant of TβRII abrogated the GFP-LC3 dot formation by TGF-β in HuH7 cells (Supplementary Fig. S4). Further, TβRI kinase inhibitors, LY364947 and SB431542, and kinase-inactive form of TβRI (ALK5-KR) attenuated autophagy activation by TGF-β (Fig. 4*A*). These results suggest the requirement of both TβRII and TβRI for TGF-β–induced autophagy.

We next examined the involvement of the Smad pathway and an autophagy inducer DAPK. GFP-LC3 dot formation by TGF-β was suppressed by knockdown of Smad4, DAPK (Fig. 4*B*), or Smad2/3 (Supplementary Fig. S5*A*). Smad4 knockdown also abolished TGF-β–induced increase of *BECLIN1*, *ATG7*, and *DAPK* but not that of *ATG5* (Fig. 5*C*). As shown in Supplementary Fig. S5*B*, GFP-LC3 dot formation by TGF-β was blocked by inhibiting mRNA synthesis

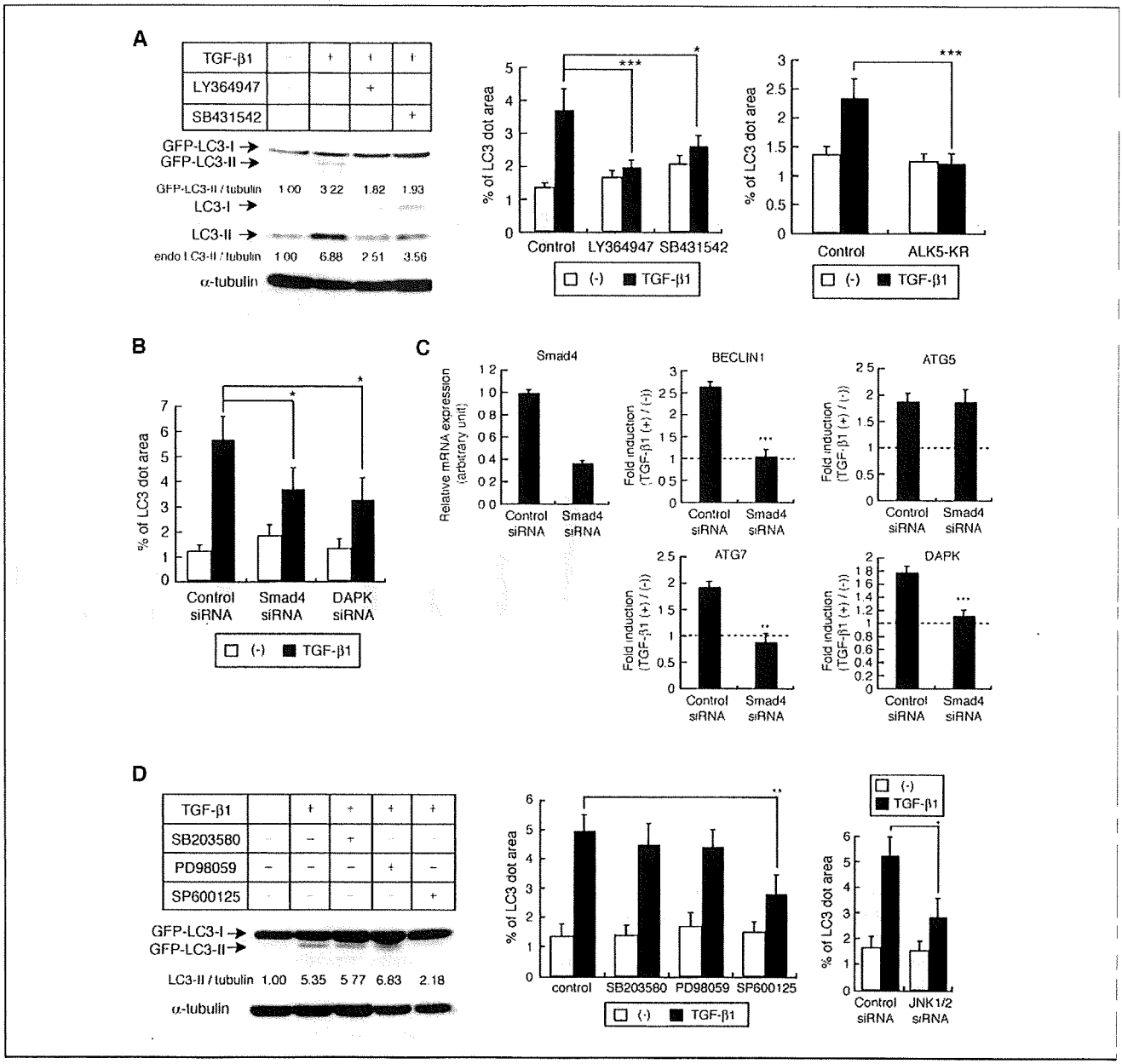

Figure 4. Involvement of TβRI, the Smad pathway, and JNK in TGF-β–regulated autophagy induction. *A*, effects of TβRI kinase inhibitors LY364947 (10 μmol/L) and SB431542 (10 μmol/L) on GFP-LC3 kinetics in HuH7 cells. The inhibitors were added 1 h before TGF-β1 treatment. LC3 conversion (*left*) and GFP-LC3 dot formation (*middle*) were analyzed after 24 and 12 h of TGF-β1 treatment, respectively. Effect of kinase-inactive TβRI (ALK5-KR) on GFP-LC3 dot formation was also determined (*right*). *, $P < 0.05$; ***, $P < 0.001$. *B*, effects of Smad4 and DAPK knockdown on GFP-LC3 dot formation by TGF-β in HuH7 cells. *, $P < 0.05$. *C*, quantitative reverse transcription-PCR analysis of ATG genes. HuH7 cells were transfected with control or Smad4 siRNA and treated with TGF-β1 (1 ng/mL, 24 h). **, $P < 0.01$; ***, $P < 0.001$. *D*, effects of MAPK inhibitors on GFP-LC3 kinetics. JNK inhibitor SP600125 (10 μmol/L), p38 MAPK inhibitor SB203580 (20 μmol/L), and extracellular signal-regulated kinase inhibitor PD98059 (10 μmol/L) were added 1 h before TGF-β1 treatment. GFP-LC3 conversion (*left*) and GFP-LC3 dot formation (*middle*) were analyzed after 24 and 12 h of TGF-β1 treatment, respectively. Effect of JNK1/2 knockdown on GFP-LC3 dot formation was also evaluated (*right*). *, $P < 0.05$; **, $P < 0.01$.

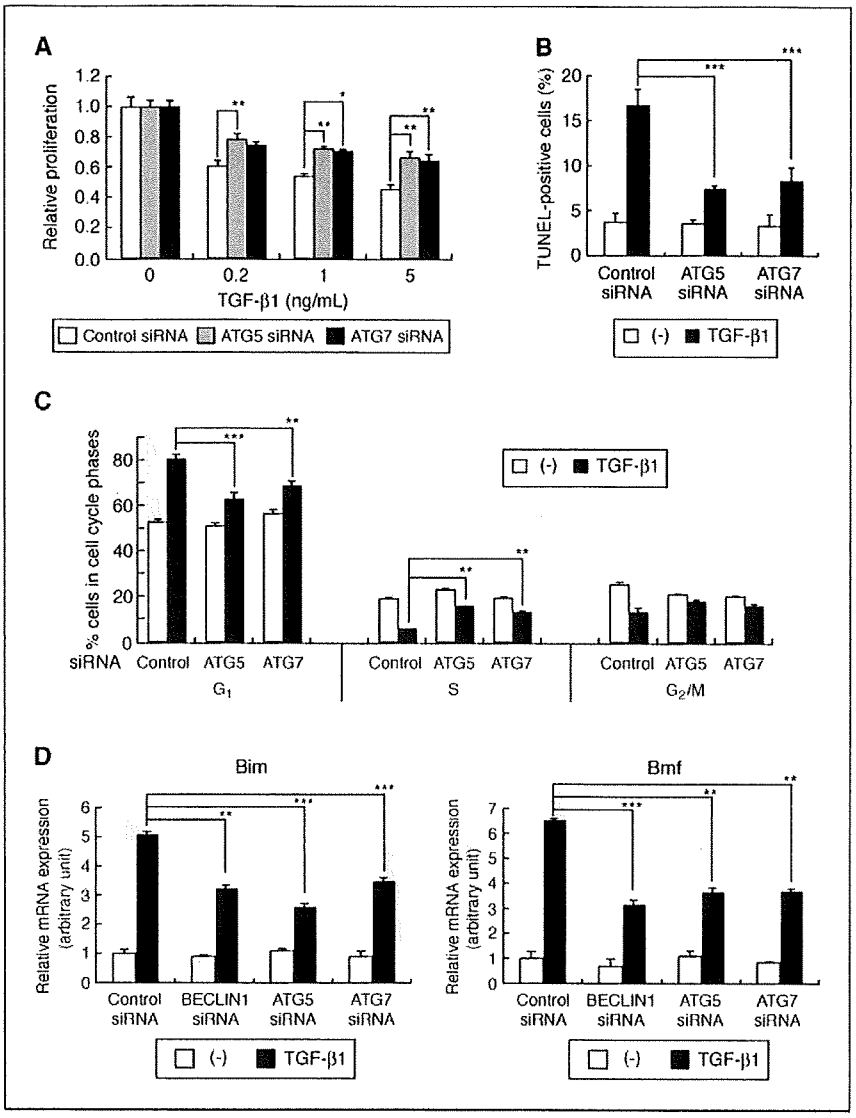

Figure 5. Inhibition of autophagy attenuates TGF-β–mediated growth inhibition and induction of Bim and Bmf. *A*, growth inhibition assay. HuH7 cells were transfected with siRNAs and treated with various doses of TGF-β1 48 h after transfection. Cell viability was determined by WST-8 assay in triplicate after 48 h. *, $P < 0.05$; **, $P < 0.01$. *B* and *C*, apoptosis assay and cell cycle analysis, respectively. After siRNA transfection and the treatment with TGF-β1 (5 ng/mL) for 48 h, assessment of apoptosis and cell cycle profiling were done. **, $P < 0.01$; ***, $P < 0.001$. *D*, quantitative reverse transcription-PCR analysis of Bim and Bmf. HuH7 cells were transfected with siRNAs and treated with TGF-β (1 ng/mL, 24 h). **, $P < 0.01$; ***, $P < 0.001$.

by actinomycin D treatment, indicating the importance of gene transcription for TGF-β–induced autophagy. Thus, the Smad pathway may regulate autophagy at least partially through the transcriptional control of autophagy-related genes. Accordingly, the degradation rate of long-lived proteins continued to increase after early activation of autophagy (6-12 h) following TGF-β treatment (Fig. 2*D*) in addition to the later increment of GFP-tagged LC3-II during the biphasic LC3-II increase (Fig. 2*A*), suggesting that TGF-β–mediated autophagy activation is sustained for a longer period after the early time-course activation. An induction of autophagy genes by TGF-β might support the sustained autophagy activation.

TGF-β also activates several non-Smad signal transduction pathways, including c-Jun NH_2-terminal kinase (JNK), p38 MAPK, and phosphoinositide 3-kinase (36). We further examined the possible involvement of non-Smad pathways. Among the MAPK inhibitors, a JNK inhibitor, SP600125, strongly inhibited TGF-β–stimulated LC3 conversion in HuH7 cells (Fig. 4*D*, *left*). We confirmed that both SP600125 treatment and JNK1/2 knockdown suppress the GFP-LC3 dot formation by TGF-β (Fig. 4*D*, *middle* and *right*; Supplementary Fig. S6*A*), suggesting an important role of JNK in the TGF-β–induced autophagy. JNK1/2 knockdown partially attenuated the TGF-β–induced increment of *BECLIN1*, *ATG7*, and *DAPK* transcripts (data not shown). Furthermore, JNK1/2 knockdown also repressed the ATG5 induction in contrast to Smad4 knockdown (Supplementary Fig. S6*B*). Because there are several crosstalks between Smad pathways and MAPK pathways including JNK (37, 38), JNK might also be positively involved in the induction of autophagy genes in addition to the Smad pathway.

Autophagy activation precedes TGF-β–induced apoptosis and blockade of ATG genes attenuates TGF-β–mediated growth inhibition. In accordance with the previous findings, cleavage of poly(ADP-ribose) polymerase became detectable after 24 h of TGF-β treatment in HuH7 cells (refs. 27, 33; Supplementary Fig. S7). Therefore, autophagy should precede the execution of apoptosis in TGF-β–treated HuH7 cells. We thus examined possible contribution of autophagy in TGF-β–mediated growth inhibition using tetrazolium-based colorimetric cell viability assay. Knockdown

of ATG5 or ATG7 by siRNA attenuated TGF-β–induced growth inhibition by ~20% in HuH7 cells (Fig. 5*A, left*).

As shown in Fig. 5*B*, ATG5 or ATG7 knockdown repressed apoptosis induced by TGF-β in HuH7 cells. Moreover, TGF-β caused the cell cycle arrest in the G_1 phase, and this cell cycle blockade was partially reverted by ATG5 or ATG7 knockdown (Fig. 5*C*). Therefore, these results suggested that the effects of autophagy inhibition on TGF-β–mediated growth inhibition are attributable to modulation of apoptosis induction and cell cycle arrest in this cell line. Taken together, we concluded that autophagy activation partially contributes to TGF-β–mediated growth inhibition in the hepatoma cells.

Autophagy regulates the TGF-β–mediated induction of the proapoptotic genes Bim and Bmf. Although the relationship between autophagy and apoptosis remains controversial and has not been well understood, a recent study showed that autophagy potentiates the Chop-dependent induction of the proapoptotic Bcl-2 family protein Bim on growth factor withdrawal and contributes to Bim-mediated apoptosis induced by growth factor deprivation in hematopoietic cells (39). Because Bim is one of the important mediators of TGF-β–induced apoptosis in hepatocytes and B lymphocytes (26, 40), we examined whether autophagy inhibition affects the induction of Bim by TGF-β. Interestingly, autophagy inhibition by knockdown of BECLIN1, ATG5, or ATG7 partially suppressed the TGF-β–mediated strong induction of *Bim* and another proapoptotic gene, *Bmf* (Fig. 5*D*), whereas the changes of other TGF-β target genes such as *p21, p15,* and *c-Myc* were not affected (data not shown). We confirmed that knockdown of Bim attenuates TGF-β–induced apoptosis in HuH7 cells (Supplementary Fig. S8), suggesting that Bim and Bmf might be candidate molecules linking autophagy to apoptosis in downstream of TGF-β signaling.

Autophagy activation by TGF-β in mammary carcinoma cells. We focused our study on TGF-β–mediated autophagy activation in hepatoma cells. Meanwhile, TGF-β has been reported

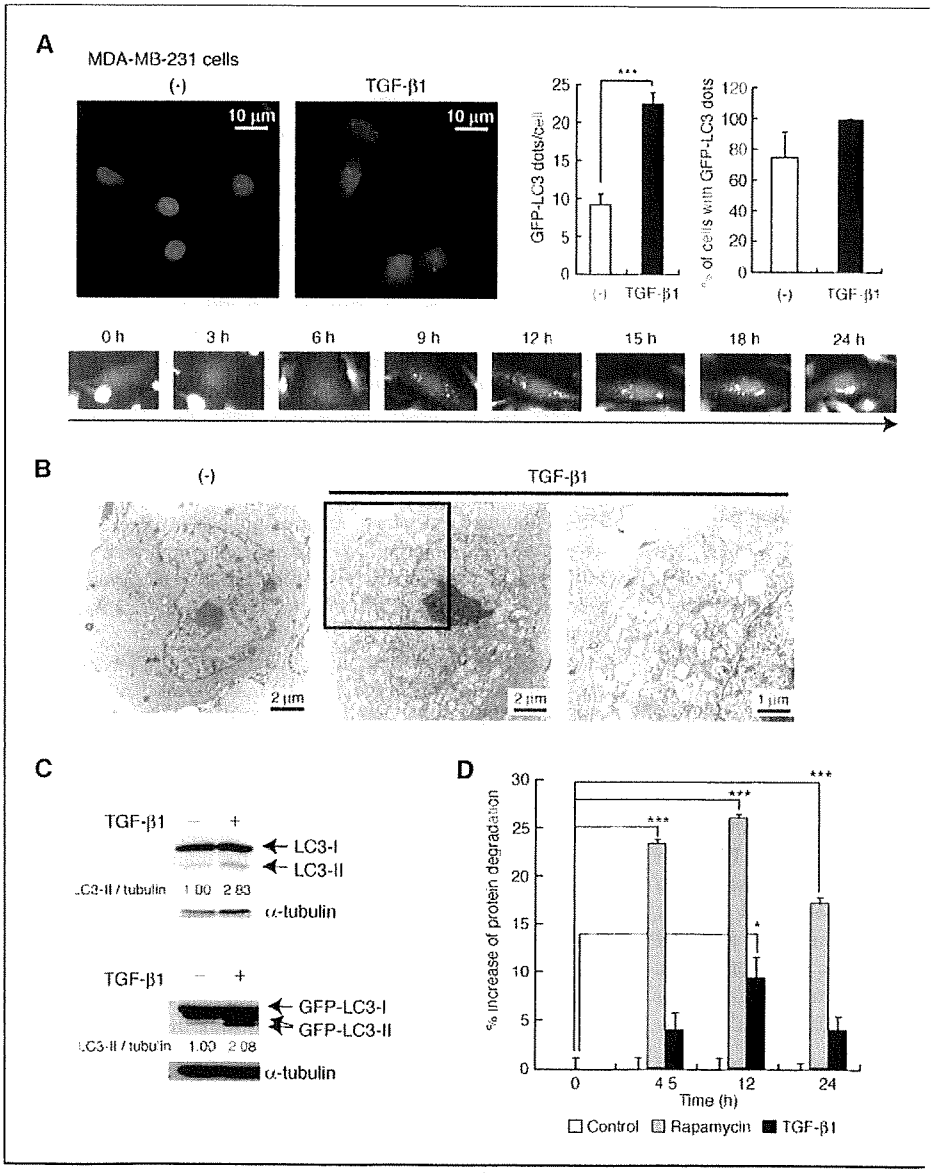

Figure 6. Autophagy is induced by TGF-β in MDA-MB-231 mammary carcinoma cells. *A*, MDA-MB-231 cells expressing GFP-LC3 were treated with TGF-β1 (1 ng/mL) for 24 h. GFP-LC3 dot formation was observed (*top left*) and quantified (*top right*) as in Fig. 1*A*. ***, $P < 0.001$. Serial change of GFP-LC3 localization was examined by video microscope (*bottom*). *B*, transmission electron microscopy. Cells were treated with TGF-β1 (1 ng/mL) for 24 h. *Right*, enlarged image of the box in the middle. *C*, conversion of endogenous LC3 (*top*) and GFP-LC3 (*bottom*) in MDA-MB-231 cells by TGF-β1 treatment (1 ng/mL, 9 h). *D*, long-lived protein degradation assay done as in Fig. 2*D*. *, $P < 0.05$; ***, $P < 0.001$.

previously to induce autophagy in normal bovine mammary epithelial BME-UV1 cells (18). Finally, we verified the potential effect of TGF-β on autophagy in mammary carcinoma cells to test whether TGF-β could induce autophagy in other types of cells. TGF-β treatment induced the formation of GFP-LC3 dots in human MDA-MB-231 mammary carcinoma cells (Fig. 6*A*, *top*). Video microscopic monitoring revealed that TGF-β induced GFP-LC3 dot formation as early as at 6 h, and the phenomena became apparent at 9 h (Fig. 6*A*, *bottom*). Transmission electron microscopy also showed the formation of autophagosomes (Fig. 6*B*). Further, TGF-β stimulated conversion of endogenous LC3 and GFP-LC3 in MDA-MB-231 cells (Fig. 6*C*) in a dose-dependent fashion (Supplementary Fig. S9*A*). TGF-β also induced GFP-LC3 conversion in mouse mammary carcinoma cell line, JygMC(A) (Supplementary Fig. S9*B*). Moreover, TGF-β enhanced degradation of long-lived proteins in MDA-MB-231 cells (Fig. 6*D*). On the other hand, the increment of protein degradation was less potent and transient than in HuH7 cells, which might be due to autophagy suppression by activated Akt signaling via K-Ras mutation in MDA-MB-231 cells (41). These results suggest that TGF-β could activate autophagy in certain mammary carcinoma cells. MDA-MB-231 cells were resistant to growth inhibition by TGF-β, and the growth-inhibitory effect could be observed only under a higher concentration of TGF-β (5 ng/mL). In such a higher concentration, the modest growth inhibition by TGF-β was suppressed by ATG5 or ATG7 knockdown (Supplementary Fig. S10).

Discussion

In the present study, we showed that TGF-β induced autophagy in certain hepatocellular carcinoma and mammary carcinoma cell lines. We found that TGF-β might induce autophagy at least partially through the Smad pathway and transcriptional activation of ATG genes. Accordingly, induction of autophagy in certain conditions such as radiation and endoplasmic reticulum stress is mediated by an increase in ATG gene transcripts (22, 42). Furthermore, a recent study showed that decreased insulin-like growth factor-I/phosphoinositide 3-kinase/Akt signaling also activates autophagy not only through mTOR but also more slowly by a transcription-dependent mechanism involving FoxO3 transcriptional factor (43). We have also found that JNK plays an important role in TGF-β–induced autophagy. p38 MAPK and JNK signaling pathways have been shown to be involved in autophagy induced by innate immune response and endoplasmic reticulum stress response (44–46). In this context, the expression of ATG5 may be regulated by the JNK pathway rather than the Smad pathway.

TGF-β has been shown to activate phosphoinositide 3-kinase/Akt/mTOR pathway during TGF-β–induced epithelial-to-mesenchymal transition (47). We observed transient phosphorylation of mTOR, a central inhibitor of autophagy, ~6 h of treatment with TGF-β in HuH7 cells (Supplementary Fig. S11). TGF-β might activate both stimulatory and inhibitory signals of autophagy, and at least in HuH7 cells, the autophagy stimulation by the Smad and JNK pathways may predominate the antiautophagic effect of mTOR. According to this hypothesis, inactivating events in TGF-β signaling pathways may influence the predisposition of tumor cells to the TGF-β–induced autophagy.

The present study shows that autophagy activation should play an important role in TGF-β–mediated growth inhibition. Although the induction of DAPK could stimulate both autophagy and apoptosis, our results show the possibility that ATG genes may additionally connect these two processes through modulation of TGF-β–mediated Bim/Bmf induction. The previous study showed that TGF-β induces transcription of *Bim* and *Bmf* in a Smad- and p38-dependent manner (40). Interestingly, we observed that TGF-β modestly induced the stress-responsive transcription factor Chop and that the induction tended to be mitigated by autophagy inhibition (data not shown). Thus, TGF-β–mediated Bim and Bmf induction could be additionally regulated in a Chop- and autophagy-dependent manner. Because autophagy has been shown to play a role in destruction of unfolded proteins, autophagy might influence the induction and activity of Chop (39). On the other hand, autophagy may play a direct role in negative growth control. In support of this notion, enforced expression of BECLIN1 attenuated the proliferation of HuH7 cells without affecting cell death (Supplementary Fig. S12) in consistence with previous studies (12, 48). This effect has been reported to be accompanied with the decrease in cyclin E expression and Rb phosphorylation (12, 48).

Autophagy plays bidirectional and paradoxical roles in tumor suppression and tumor progression (14). Autophagy was initially described as a cytoprotective mechanism under nutrient deprivation, although several lines of evidence documented a role for autophagy in promoting cell death, similar to the results of our study observed in HuH7 cells. This discrepancy may be partially explained by the presumption that extensive autophagy activation contributes to cell death, and autophagy induction within restricted ranges supports cell survival (14). From this view, we observed that TGF-β activates autophagy more potently and continuously in HuH7 hepatoma cells than in MDA-MB-231 breast cancer cells (compared by the results of enhanced long-lived protein degradation by TGF-β; Figs. 2*D* and 6*D*). On the other hand, TGF-β induces cell cycle arrest and apoptosis in hepatoma cells (26, 27), but the effects were mitigated in breast cancer cells and TGF-β promotes cell survival of breast cancer cells in other settings (23). Considering the magnitude of autophagy induction and context-dependent growth-inhibitory effect of TGF-β, we thus speculated that higher and prolonged autophagy induction contributes to TGF-β–mediated growth inhibition in hepatoma cells. Although the role of TGF-β–induced autophagy remains unclear in breast cancer cells, lower activation of autophagy in a restricted manner might support TGF-β–mediated cell survival mechanism(s), particularly in cancer cells in which the apoptotic responses such as Bim induction are compromised.

In addition, the role of autophagy might be different in certain stages and aspects in tumor development. Various tumor suppressors (e.g., PTEN, TSC1/2, p53, and DAPK) are autophagy inducers, whereas some inhibitors of autophagy (e.g., Akt and Ras) possess oncogenic activity (49). One of the early stages in tumorigenesis is oncogenic transformation, which is achieved by the loss of such tumor suppressors and activation of oncogenic pathways. In this setting, autophagy may be involved in the maintenance of genomic stability for tumor suppression (15). Because TGF-β primarily functions as a tumor suppressor in early stages of carcinogenesis, TGF-β–induced autophagy may suppress tumor initiation in cooperation with other tumor suppressors. In later stages of tumor progression, it was shown that the metabolically stressed regions of the tumor mass activate autophagy (50). In this scenario, autophagy activation might confer a growth advantage to these cells. Regarding the tumor-promoting aspects of TGF-β in advanced cancer, TGF-β–induced autophagy in certain tumor types including breast cancer might be thus implicated in tumor promotion in the later phase of tumorigenesis.

In conclusion, we showed that TGF-β stimulates autophagy flux in certain human cancer cells at least partially through the increased expression of some ATG genes and that not only the Smad but also the JNK pathway are involved in this process. Furthermore, autophagy has been shown to play an important role in the TGF-β–induced growth inhibition in hepatocellular carcinoma cells. The involvement of autophagy induction in relation to the tumor-suppressive and tumorigenic effects of TGF-β should be further investigated in the future. Induction of autophagy should participate in various biological activities of TGF-β, and elucidation of its molecular mechanism will bring a better understanding of both physiologic and pathologic effects of TGF-β signaling pathways.

Disclosure of Potential Conflicts of Interest

No potential conflicts of interest were disclosed.

Acknowledgments

Received 11/19/08; revised 9/1/09; accepted 9/24/09; published OnlineFirst 11/10/09.

Grant support: KAKENHI (Grant-in-Aid for Scientific Research) and Global Center of Excellence Program for "Integrative Life Science Based on the Study of Biosignaling Mechanisms" from the Ministry of Education, Culture, Sports, Science and Technology of Japan.

The costs of publication of this article were defrayed in part by the payment of page charges. This article must therefore be hereby marked *advertisement* in accordance with 18 U.S.C. Section 1734 solely to indicate this fact.

We thank M. Oka, C. Iwata, and S. Ehata for discussion, Y. Hoshino for technical advice, T. Yoshimori (Osaka University) for the GFP-LC3 vector, and all members of Department of Molecular Pathology, University of Tokyo.

References

1. Mizushima N. Autophagy: process and function. Genes Dev 2007;21:2861–73.
2. Mathew R, Karantza-Wadsworth V, White E. Role of autophagy in cancer. Nat Rev Cancer 2007;7:961–7.
3. Kroemer G, Jaattela M. Lysosomes and autophagy in cell death control. Nat Rev Cancer 2005;5:886–97.
4. Kondo Y, Kanzawa T, Sawaya R, Kondo S. The role of autophagy in cancer development and response to therapy. Nat Rev Cancer 2005;5:726–34.
5. Maiuri MC, Zalckvar E, Kimchi A, Kroemer G. Self-eating and self-killing: crosstalk between autophagy and apoptosis. Nat Rev Mol Cell Biol 2007;8:741–52.
6. Komatsu M, Waguri S, Chiba T, et al. Loss of autophagy in the central nervous system causes neurodegeneration in mice. Nature 2006;441:880–4.
7. Lee HK, Iwasaki A. Autophagy and antiviral immunity. Curr Opin Immunol 2008;20:23–9.
8. Levine B, Klionsky DJ. Development by self-digestion: molecular mechanisms and biological functions of autophagy. Dev Cell 2004;6:463–77.
9. Klionsky DJ, Cregg JM, Dunn WA, Jr., et al. A unified nomenclature for yeast autophagy-related genes. Dev Cell 2003;5:539–45.
10. Karantza-Wadsworth V, Patel S, Kravchuk O, et al. Autophagy mitigates metabolic stress and genome damage in mammary tumorigenesis. Genes Dev 2007;21:1621–35.
11. Aita VM, Liang XH, Murty VV, et al. Cloning and genomic organization of beclin 1, a candidate tumor suppressor gene on chromosome 17q21. Genomics 1999;59:59–65.
12. Liang XH, Jackson S, Seaman M, et al. Induction of autophagy and inhibition of tumorigenesis by beclin 1. Nature 1999;402:672–6.
13. Qu X, Yu J, Bhagat G, et al. Promotion of tumorigenesis by heterozygous disruption of the beclin 1 autophagy gene. J Clin Invest 2003;112:1809–20.
14. Eisenberg-Lerner A, Kimchi A. The paradox of autophagy and its implication in cancer etiology and therapy. Apoptosis 2009;14:376–91.
15. Mathew R, Kongara S, Beaudoin B, et al. Autophagy suppresses tumor progression by limiting chromosomal instability. Genes Dev 2007;21:1367–81.
16. Wakefield LM, Roberts AB. TGF-β signaling: positive and negative effects on tumorigenesis. Curr Opin Genet Dev 2002;12:22–9.
17. Bierie B, Moses HL. Tumour microenvironment: TGFβ: the molecular Jekyll and Hyde of cancer. Nat Rev Cancer 2006;6:506–20.
18. Gajewska M, Gajkowska B, Motyl T. Apoptosis and autophagy induced by TGF-β1 in bovine mammary epithelial BME-UV1 cells. J Physiol Pharmacol 2005;56 Suppl 3:143–57.
19. Kabeya Y, Mizushima N, Ueno T, et al. LC3, a mammalian homologue of yeast Apg8p, is localized in autophagosome membranes after processing. EMBO J 2000;19:5720–8.
20. Shibuya K, Shirakawa J, Kameyama T, et al. CD226 (DNAM-1) is involved in lymphocyte function-associated antigen 1 costimulatory signal for naive T cell differentiation and proliferation. J Exp Med 2003;198:1829–39.
21. Amaravadi RK, Yu D, Lum JJ, et al. Autophagy inhibition enhances therapy-induced apoptosis in a Myc-induced model of lymphoma. J Clin Invest 2007;117:326–36.
22. Apel A, Herr I, Schwarz H, Rodemann HP, Mayer A. Blocked autophagy sensitizes resistant carcinoma cells to radiation therapy. Cancer Res 2008;68:1485–94.
23. Ehata S, Hanyu A, Hayashi M, et al. Transforming growth factor-β promotes survival of mammary carcinoma cells through induction of antiapoptotic transcription factor DEC1. Cancer Res 2007;67:9694–703.
24. Franch HA, Sooparb S, Du J, Brown NS. A mechanism regulating proteolysis of specific proteins during renal tubular cell growth. J Biol Chem 2001;276:19126–31.
25. Furuta S, Hidaka E, Ogata A, Yokota S, Kamata T. Ras is involved in the negative control of autophagy through the class I PI3-kinase. Oncogene 2004;23:3898–904.
26. Sanchez-Capelo A. Dual role for TGF-β1 in apoptosis. Cytokine Growth Factor Rev 2005;16:15–34.
27. Lin JK, Chou CK. *In vitro* apoptosis in the human hepatoma cell line induced by transforming growth factor β1. Cancer Res 1992;52:385–8.
28. Kuma A, Matsui M, Mizushima N. LC3, an autophagosome marker, can be incorporated into protein aggregates independent of autophagy: caution in the interpretation of LC3 localization. Autophagy 2007;3:323–8.
29. Tanida I, Minematsu-Ikeguchi N, Ueno T, Kominami E. Lysosomal turnover, but not a cellular level, of endogenous LC3 is a marker for autophagy. Autophagy 2005;1:84–91.
30. Mizushima N, Yoshimori T. How to interpret LC3 immunoblotting. Autophagy 2007;3:542–5.
31. Yu L, Alva A, Su H, et al. Regulation of an ATG7-beclin 1 program of autophagic cell death by caspase-8. Science 2004;304:1500–2.
32. Klionsky DJ, Abeliovich H, Agostinis P, et al. Guidelines for the use and interpretation of assays for monitoring autophagy in higher eukaryotes. Autophagy 2008;4:151–75.
33. Jang CW, Chen CH, Chen CC, Chen JY, Su YH, Chen RH. TGF-β induces apoptosis through Smad-mediated expression of DAP-kinase. Nat Cell Biol 2002;4:51–8.
34. Harrison B, Kraus M, Burch L, et al. DAPK-1 binding to a linear peptide motif in MAP1B stimulates autophagy and membrane blebbing. J Biol Chem 2008;283:9999–10014.
35. Ozdamar B, Bose R, Barrios-Rodiles M, Wang HR, Zhang Y, Wrana JL. Regulation of the polarity protein Par6 by TGFβ receptors controls epithelial cell plasticity. Science 2005;307:1603–9.
36. Moustakas A, Heldin CH. Non-Smad TGF-β signals. J Cell Sci 2005;118:3573–84.
37. Guo B, Inoki K, Isono M, et al. MAPK/AP-1-dependent regulation of PAI-1 gene expression by TGF-β in rat mesangial cells. Kidney Int 2005;68:972–84.
38. Yang C, Patel K, Harding P, Sorokin A, Glass WF II. Regulation of TGF-β1/MAPK-mediated PAI-1 gene expression by the actin cytoskeleton in human mesangial cells. Exp Cell Res 2007;313:1240–50.
39. Altman BJ, Wofford JA, Zhao Y, et al. Autophagy provides nutrients but can lead to Chop-dependent induction of Bim to sensitize growth factor-deprived cells to apoptosis. Mol Biol Cell 2009;20:1180–91.
40. Ramjaun AR, Tomlinson S, Eddaoudi A, Downward J. Upregulation of two BH3-only proteins, Bmf and Bim, during TGF β-induced apoptosis. Oncogene 2007;26:970–81.
41. Toulany M, Baumann M, Rodemann HP. Stimulated PI3K-AKT signaling mediated through ligand or radiation-induced EGFR depends indirectly, but not directly, on constitutive K-Ras activity. Mol Cancer Res 2007;5:863–72.
42. Kouroku Y, Fujita E, Tanida I, et al. ER stress (PERK/eIF2α phosphorylation) mediates the polyglutamine-induced LC3 conversion, an essential step for autophagy formation. Cell Death Differ 2007;14:230–9.
43. Zhao J, Brault JJ, Schild A, et al. FoxO3 coordinately activates protein degradation by the autophagic/lysosomal and proteasomal pathways in atrophying muscle cells. Cell Metab 2007;6:472–83.
44. Li C, Capan E, Zhao Y, et al. Autophagy is induced in CD4$^+$ T cells and important for the growth factor-withdrawal cell death. J Immunol 2006;177:5163–8.
45. Xu Y, Jagannath C, Liu XD, Sharafkhaneh A, Kolodziejska KE, Eissa NT. Toll-like receptor 4 is a sensor for autophagy associated with innate immunity. Immunity 2007;27:135–44.
46. Ogata M, Hino S, Saito A, et al. Autophagy is activated for cell survival after endoplasmic reticulum stress. Mol Cell Biol 2006;26:9220–31.
47. Lamouille S, Derynck R. Cell size and invasion in TGF-β-induced epithelial to mesenchymal transition is regulated by activation of the mTOR pathway. J Cell Biol 2007;178:437–51.
48. Koneri K, Goi T, Hirono Y, Katayama K, Yamaguchi A. Beclin 1 gene inhibits tumor growth in colon cancer cell lines. Anticancer Res 2007;27:1453–7.
49. Botti J, Djavaheri-Mergny M, Pilatte Y, Codogno P. Autophagy signaling and the cogwheels of cancer. Autophagy 2006;2:67–73.
50. Degenhardt K, Mathew R, Beaudoin B, et al. Autophagy promotes tumor cell survival and restricts necrosis, inflammation, and tumorigenesis. Cancer Cell 2006;10:51–64.

Laboratory Investigation (2009) 89, 645–656

Human synovial sarcoma proto-oncogene Syt is essential for early embryonic development through the regulation of cell migration

Taichi Kimura[1], Mieko Sakai[1], Kouichi Tabu[1], Lei Wang[1], Ryosuke Tsunematsu[2], Masumi Tsuda[3], Hirofumi Sawa[1,*], Kazuo Nagashima[1,†], Hiroshi Nishihara[1], Shigetsugu Hatakeyama[4], Keiko Nakayama[5], Marc Ladanyi[6], Shinya Tanaka[1] and Keiichi I Nakayama[2]

SYT–SSX protein, resulted from chromosomal translocation, causes synovial sarcoma, which is a malignant tumor accounting for 10% of soft tissue sarcoma. However, biological functions of SYT (synovial sarcoma translocation), also known as SS18, are largely unclear, whereas it has been proven that *Syt*-null mice die at early stages of embryonic development. Here, we generated *Syt*-deficient mice and confirmed the reported phenotypes, including growth retardation, open neural tube and haplo-insufficient lethality, and therefore, there is no doubt that Syt is essential for embryonic development. However, placental defects, described in the earlier report, were rarely seen in our mice and we frequently observed cardiac defect in *Syt*-deficient mice. As the mechanisms responsible for embryonic lethality seem to be complicate, we performed additional experiments. By using primary cultured embryonic fibroblasts, we showed that $Syt^{-/-}$ MEFs deregulate actin organization and suppressed cell migration. These observations suggest that Syt may contribute to the signaling pathway important for various cellular functions *in vivo* and *in vitro*, and we propose that *Syt*-deficient MEFs would be a powerful means to understand the biological roles of SYT *in vitro*.
Laboratory Investigation (2009) **89,** 645–656; doi:10.1038/labinvest.2009.25; published online 30 March 2009

KEYWORDS: Syt; p300; synovial sarcoma; embryonic lethality; cardiogenesis; motility

Human synovial sarcoma is an aggressive tumor that accounts for almost 10% of all soft tissue sarcomas and typically arises in the para-articular regions in young adults.[1,2] Synovial sarcoma possesses a specific chromosomal translocation between chromosomes (chr) 18 and X, forming a chimeric gene fusing SYT (synovial sarcoma translocation) on chr 18 to SSX (synovial sarcoma X break point) on chr X.[3] The translocation found in synovial sarcoma removes the last eight amino acids of SYT and fuses it to the C-terminal portion of the SSX to yield a SYT–SSX fusion protein.[3] In contrast to SSX, which is thought to act as a transcriptional regulator because of its sequence homology to other transcription repressors, SYT does not share a homologous region or conserved domain with other human proteins.[4]

SYT is a ubiquitously expressed nuclear protein containing two distinct domains. One is the SYT amino N-terminal homology domain, which shows homology to the predicted proteins of EST clones derived from a wide variety of species, and the other is the carboxy C-terminal QPGY domain, which is rich in glutamine, proline, glycine and tyrosine.[5] The QPGY domain was shown to activate the transcription of a reporter gene when it was fused to a DNA-binding domain.[5,6] As SYT lacks a DNA-binding domain, it may function as a transcriptional co-activator.[6] In fact, SYT has been shown to

[1]Laboratory of Molecular and Cellular Pathology, Graduate School of Medicine, Hokkaido University, Sapporo, Japan; [2]Department of Molecular and Cellular Biology, Medical Institute of Bioregulation, Kyushu University, Fukuoka, Fukuoka, Japan; [3]Department of Laboratory Medicine, Hokkaido University Graduate School of Medicine, Sapporo, Japan; [4]Department of Molecular Biochemistry, Hokkaido University Graduate School of Medicine, Sapporo, Japan; [5]Department of Developmental Biology, Center for Translational and Advanced Animal Research on Human Disease, Graduate School of Medicine, Tohoku University, Aobaku, Sendai, Japan and [6]Department of Pathology, Memorial Sloan-Kettering Cancer Center, New York, NY, USA
Correspondence: Professor S Tanaka, MD, PhD, Laboratory of Molecular and Cellular Pathology, Hokkaido University School of Medicine, N 15, W 7, Kita-ku, Sapporo 060-8638, Japan.
E-mail: tanaka@med.hokudai.ac.jp
*Current address: Hirofumi Sawa, Department of Pathobiology, Hokkaido University Zoonosis Research Center, and 21st Century COE Program for Zoonosis Control, N12, W9, Sapporo, Japan
†Current address: Kazuo Nagashima, Sapporo Higashi Tokushukai Hospital, N33, E13, Sapporo, Japan
Received 25 January 2009; revised 22 February 2009; accepted 27 February 2009

bind to hBRM/hSNF2α, a major component of the SWI/SNF-type chromatin remodeling complex.[5,7–9] Moreover, it was also shown that SYT interacts with the putative transcriptional factor AF10, histone acetyl transferase p300 and a component of histone deacetylase complex mSin3A.[10–12] Thus, it is possible that SYT regulates transcription through the binding to chromatin modifiers. In spite of these biochemical studies of SYT, the physiological function of SYT remains largely unknown.

To examine the role of SYT *in vivo*, we established *Syt*-deficient mice by a gene targeting strategy. $Syt^{-/-}$ homozygous mutant mice died around mid-gestation and exhibited multiple defects in morphogenesis. These results support the essential gene dosage-sensitive role of Syt in embryogenesis. Subsequently, to examine cellular basis of these phenotypes, we established MEFs from wild-type and $Syt^{-/-}$ at E9.75. We found that the absence of Syt affects cell migration. These results suggest that SYT plays an important role in cellular motility through the regulation of cytoskeletal organization.

MATERIALS AND METHODS

Generation of Syt Knockout Mice

A targeting vector, designed to delete exons 1 and 2 of the Syt gene, was constructed using a PKG-lox-Neo-poly(A) cassette as described earlier.[13] Briefly, the targeted embryonic stem cell clone was microinjected into host blastocysts, and the resulting chimeric mice were C57BL/6 mice to achieve germ-line transmission of the *Syt* mutation. The mice used in this study were of mixed genetic background (129/Sv and C57BL/6).

Genotyping of Mice

Genomic DNA samples (15 μg) isolated from 3-week-old mice were digested with *Eco*RV and *Spe*I and analyzed by Southern blotting. A probe for Southern blotting was generated by genomic PCR. Primer sequences used in this experiment included 5′-TTACAGAGGATTGGGAAAGG-3′ and 5′-CTGGTATTTCGCTAAGGAAG-3′. Routine genotyping of mice was performed by PCR using three primers: F 5′-GAG TCC TGC CTG GGA TGA GAA C-3′, R 5′-CGA TAG AAG ATG AAG ACT CTG GCC -3′ and PJL 5′-TGC TAA AGC GCA TGC TCC AGA CTG T-3′, which resulted in 453-bp (F/R) and 370-bp (F/PJL) products from wild-type and targeted alleles, respectively.

Histopathological and Immunohistochemical Analysis

Embryos were fixed with 4% paraformaldehyde in phosphate-buffered saline and embedded in paraffin. Four-μm tissue sections were deparaffinized with xylene and rehydrated through a graded ethanol series and subjected to hematoxylin and eosin stain. Histopathological examination was performed by trained histopathologists. For immunohistochemical analysis, antigens were retrieved in citrate buffer (pH 6.0) by using a pressure cooker. Then, sections were incubated with 0.3% H_2O_2 in methanol to quench endogenous peroxidase activity and then treated with normal rabbit or goat serum to eliminate nonspecific binding of the antibodies. After treatment, sections were incubated with primary antibodies for PCNA (M879; DakoCytomation, CA, USA), hBRM (a gift from Yasunori Machida in Nagoya University, Japan), BRG1 (a gift from Yasunori Machida in Nagoya University, Japan) and mSYT (generated in our lab) at 4°C overnight. After incubation with the biotinylated secondary antibody, immunoreaction products were visualized with enzymatic reaction of peroxidase, with 3, 3′-diaminobenzidine tetrahydrochloride (DAB) as a substrate.

Terminal Deoxynucleotidyltransferase-Mediated dUTP-Biotin Nick End Labeling Assay

Paraffin-embedded tissue sections were deparaffinized and washed with 0.1 M phosphate buffer for a few minutes, and permeabilized for 20 min at room temperature (RT) with proteinase K (20 μg/ml in 0.1 M phosphate buffer) and bleached with 2% H_2O_2 for 7 min at RT. Thereafter, the samples were washed with terminal deoxynucleotidyl transferase (TdT) buffer composed of 30 mM Tris-HCl (pH 7.2), 140 mM sodium cacodylate and 1 mM cobalt chloride, and incubated for 90 min at RT with TdT reaction mixture containing TdT and biotinylated dUTP in TdT buffer. Labeled DNA was visualized with enzymatic reaction of peroxidase and DAB.

Electron Microscopic Analysis

Embryos were fixed with 2.5% glutaraldehyde (TAAB; Laboratory Equipment, Aldermaston, UK) in 0.1 M phosphate buffer at 4°C for 40 h, and then washed with 7% sucrose in 0.1 M phosphate buffer. Thereafter, the samples were fixed with 1% OsO_4 (Next Chimica, South Africa) in 0.1 M phosphate buffer at RT for 90 min and gradually dehydrated with 50, 70 and 95% acetone in ethanol for 15 min each; 95% acetone for 15 min; and 100% acetone three times for 20 min each. Afterward, the samples were treated with epon solution containing 60% solution A (a mixture of 62 ml of epon 812 (TAAB) and 100 ml of dodecenyl succinic anhydride) and 40% solution B (a mixture of 100 ml of epon 812 and 89 ml of methyl nadic anhydride). The samples were treated with epon/acetone (1:1) overnight, epon/acetone (3:1) for 1 h and epon solution for 1 h, and embedded in epon with 1.5% 2, 4, 6-tri(dimethylaminomethyl)phenol in a capsule (Nissin EM, Tokyo, Japan). The embedded samples were sectioned on an ultramicrotome at 0.1-μm thickness, put onto a grid (TAAB) and treated with 1.5% uranyl acetate (Merk, Darmstadt, Germany) for 20 min and 0.2% lead citrate (Kishida Chemistry, Tokyo, Japan) for 15 min. Finally, the samples were observed with an electron microscope (Hitachi 7100, Tokyo, Japan).

Immunoblot Analysis

Immunoblotting was performed according to a standard protocol described elsewhere.[14] Briefly, embryos were lysed with lysis buffer composed of 50 mM Tris-HCl (pH 7.6), 150 mM NaCl, 0.5% Triton X-100, 1 mM PMSF and 1 mM Na_3VO_4, and clarified by microcentrifugation at 12 000 *g* for 10 min at 4°C. Supernatants containing 20 μg of proteins were subjected to SDS-PAGE, and separated proteins were transferred to PVDF filters. The filters were blocked with 5% skim milk and incubated with primary antibodies for hBRM, BRG1, p300 (N-15; Santa Cruz Biotechnology, CA, USA), mSYT and α-tubulin (B-5-1-2; Sigma, MI, USA). Antibody binding was visualized by chemiluminescence (ELC; Amersham Pharmacia Biotech, NJ, USA).

RNA Extraction, Labeling and Hybridization

For microarray analysis, RNA was isolated from embryos or MEFs using the RNeasy mini kit (Qiagen, CA, USA). For microarray studies, labeling and hybridization were performed according to Affymetrix standard protocols. Labeled cRNA was hybridized onto the Affymetrix GeneChip Mouse Genome 430A 2.0 array (Affymetrix, CA, USA), which contains 22 691 probes. Microarray slides were scanned using the Affymetrix GCS 2500 scanner to collect fluorescence signal.

Preparation of MEFs and Cell Cultures

Primary MEFs were obtained from 9.75 d.p.c. embryos that were either wild-type or $Syt^{-/-}$ using established procedure.[15] Cells were cultured at 37°C (6% CO_2) in MEF medium (Dulbecco's modified Eagle's medium containing 10% fetal bovine serum supplemented with 2 mM L-glutamine, 0.1 mM sodium pyruvate, 0.1 mM MEM nonessential amino-acid solution, 100 U/ml penicillin G, 100 μg/ml streptomycin and 50 μM 2-mercaptoethanol).

Immunocytofluorescence and Confocal Microscopy

Wild-type and $Syt^{-/-}$ MEFs were grown on Lab-Tek chamber slides (Nalge Nunc, NY, USA) in MEF medium, were fixed with 3% paraformaldehyde in PBS for 15 min, permeabilized with 0.5% Triton X-100 in PBS for 5 min and incubated with 1% bovine serum albumin in PBS for 20 min at RT. They were then incubated overnight at 4°C with mouse monoclonal antibodies specific for paxillin (1:2000; BD Transduction Laboratories, CA, USA), then for 1 h at RT with Alexa Fluor 488-conjugated secondary antibodies (Molecular Probes, OR, USA) and finally for 30 min at RT with Alexa Fluor 594-conjugated phalloidin (Molecular Probes). The cells were then examined with a confocal laser-scanning microscope equipped with a computer (MRC-1024; Bio-Rad Microscience, CA, USA).

Wound Closure Assay

The wound closure assay was performed as described.[16] Wild-type and $Syt^{-/-}$ MEFs were grown in MEF medium for 48 h. The confluent cells were wounded by scratching the monolayer with a pipette tip, washed twice with PBS, allowed to migrate in MEF medium for the indicated times and photographed. The assay was performed in triplicate.

Semi-Quantitative Reverse Transcription PCR Analysis

Total RNA was isolated from wild-type and $Syt^{-/-}$ MEFs using RNeasy mini kit (Qiagen) according to the manufacturer's instruction. Reverse transcription was carried out with Superscript II RT (Invitrogen, CA, USA) according to the manufacturer's instruction. One hundred nanograms of the resulting first-strand cDNA was used as template and amplified by PCR using KOD-Plus DNA polymerase (Toyobo, Osaka, Japan). Sequences of the oligonucleotide primer sets used for reverse transcription PCR (RT-PCR) analysis are as follows: CD44: forward 5′-GCA CCC CAG AAG GCT ACA TTT-3′, reverse 5′-TCT GCC CAC ACC TTC TCC TAC TAT-3′; FoxG1: forward 5′-CAG CAC TTT GAG TTA CAA CG-3′, reverse 5′-TGG TCT GCG AAG TCA TTG AC-3′; HMGA2: forward 5′-AAC CTT ACT GGG TCG GCA TC-3′, reverse 5′-GGT GAG GTT TGA GCT CCT TC-3′; IGFR2: forward 5′-CAG GTA GCG AAA AGT GGT AAG T-3′, reverse 5′-GCC TGG TCT GTT TCT GTG ATT G-3′; Neuropilin: forward 5′-GAA TGT TGG GCA TGG TGT CT-3′; reverse 5′-CTT AGCCTTGCGCTTGCT-3′; Neurotrophin3: forward 5′-AAA ACC GGT AAC TCT CCT GTG-3′, reverse 5′-CTA CGA GTT TGT TGT TTT CTG-3′, PDGFRB: forward 5′-AGG TCA TTG AGT CTG TGA GC-3′, reverse 5′-ATC GGC AGT ATT CCG TGA TG-3′; Pleiotrophin: forward 5′-ACT GGC GCC GAG TGC AAACAG-3′, reverse 5′-GAG CTT GCC ACA GGG CTT GGA-3′; RGEF4: forward 5′-GCC TAT TCG TGG CTC TG-3′, reverse 5′-CAGACCTCAGTGACAACC-3′; RUNX2: forward 5′-CTC TGG CCT TCC TCT CTC AGT AA-3′, reverse 5′-TAG GTA AAG GTG GCT GGG TAG TG-3′; SDF1: forward 5′-ACT TTC CCT CTC GGT CCA C-3′, reverse 5′-TTG TTT AAA GCT TTC TCC AGG TA-3′; TCF-4: forward 5′-GGG GCT CAT ACT CAT CTT-3′, reverse 5′-GCC TGT CCT CCA TTT CTA-3′; GAPDH: forward 5′-GTC GTG GAG TCT ACT GGT GTC-3′, reverse 5′-GAG CCC TTC CAC AAT GCC AAA-3′.

RESULTS

Generation of Syt-Deficient Mice

A targeting vector containing a Neo cassette was used to replace the 5.2-kb genomic sequence of *Syt* gene including exon 1and exon 2 through homologous recombination (Figure 1a). Southern blot analysis using tail DNA from 3-week-old mice confirmed that Syt $^{+/-}$ mouse carried targeted allele (Figure 1b). Targeting of the *Syt* gene was also confirmed by immunohistochemistry and immunoblotting using E10.5 mouse embryos (Figure 1c and d). Heterozygous embryos seemed to express less amount of Syt protein than wild-type embryos (Figure 1d).

To date, none of the $Syt^{-/-}$ homozygous mutant has been detected among the 202 newborns from heterozygote crosses. $Syt^{+/-}$ heterozygous offspring appeared to be normal and

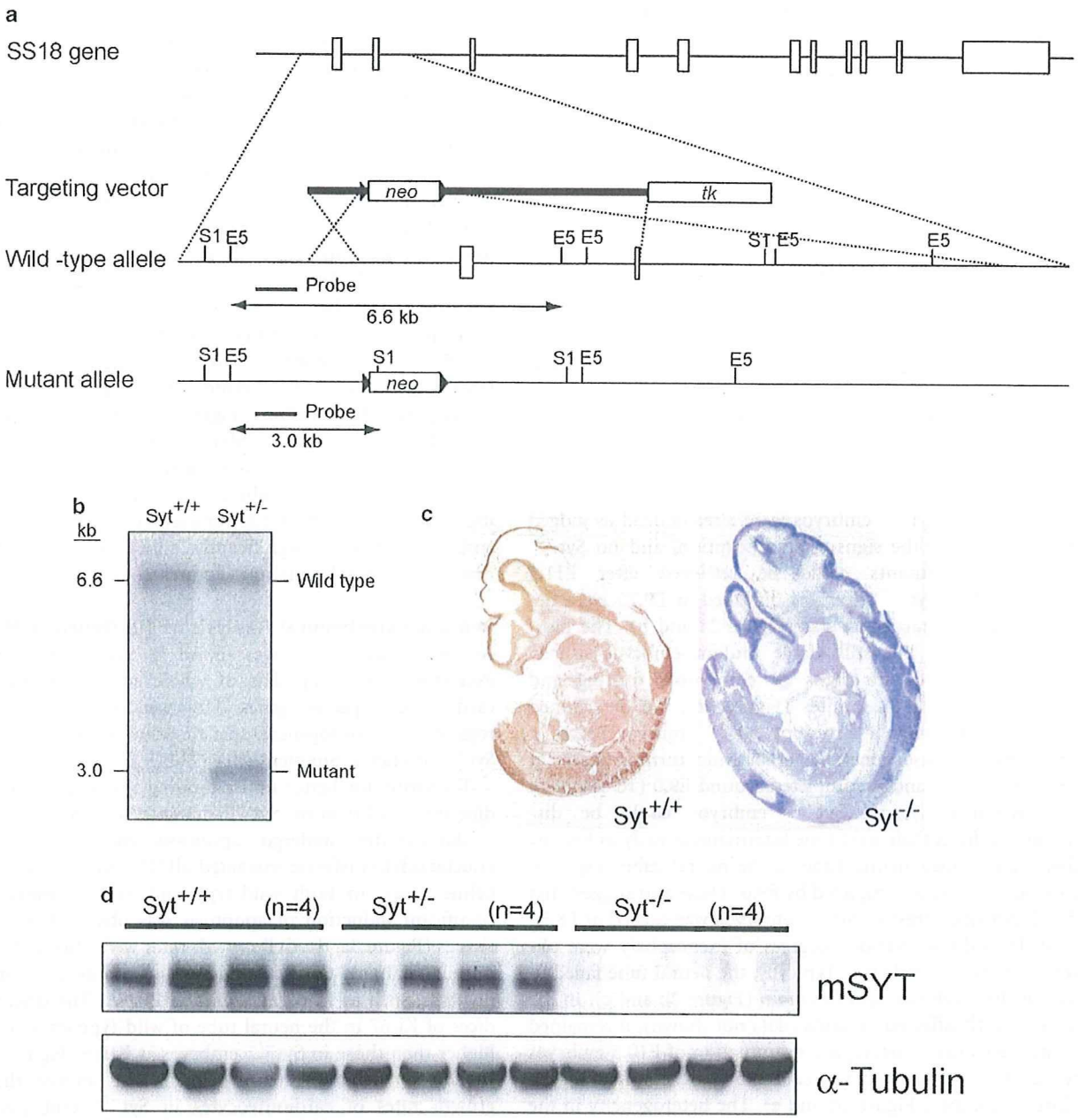

Figure 1 Targeting disruption of the Syt locus and the establishment of a mutant mouse strain. (**a**) Schematic representation of the wild-type allele, targeting vector and targeted allele. The open boxes on the alleles represent the exons. A Neo cassette replaced exons 1 and 2 of the *Syt* gene. The expected sizes of the *Eco*RV (E5) and *Spe*I (S1) digestion products of the gene, hybridized with the indicated probe, are shown. (**b**) Genomic DNA isolated from 3-week-old mice was digested with *Eco*RV and *Spe*I, and analyzed by Southern blotting with the probe shown in (**a**). (**c**) Wild-type (left) and homozygous (right) E10.5 embryos were subjected to immunohistochemistry using an anti-mSYT antibody. (**d**) Protein extracts (30 μg) from wild-type (lanes 1–4), heterozygous (lanes 5–8) and homozygous E10.5 embryos (lanes 9–12) were analyzed by immunoblotting using an anti-mSYT antibody.

fertile. The rate of $Syt^{+/-}$ heterozygous mutants among newborns was 38% lower than that expected by Mendelian inheritance (Table 1). As no neonatal lethality was observed, a certain population of $Syt^{+/-}$ heterozygous embryos must have died very early *in utero*.

Histopathological Examination of Syt-Deficient Mice

To determine the time point at which the $Syt^{-/-}$ mutant embryos become lethal, we examined embryos from $Syt^{+/-}$ intercrosses at various developmental stages. Most of $Syt^{-/-}$ homozygous embryos were alive at E9.5. At E10.5, approxi-